

Modulation of Arctic Sea Ice Loss by Atmospheric Teleconnections from Atlantic Multidecadal Variability

FREDERIC S. CASTRUCCIO

Climate and Global Dynamics Laboratory, National Center for Atmospheric Research, Boulder, Colorado

YOHAN RUPRICH-ROBERT

Barcelona Supercomputing Center, Barcelona, Spain

STEPHEN G. YEAGER AND GOKHAN DANABASOGLU

Climate and Global Dynamics Laboratory, National Center for Atmospheric Research, Boulder, Colorado

RYM MSADEK

Centre National de la Recherche Scientifique/Centre Européen de Recherche et de Formation Avancée en Calcul Scientifique, CECI UMR 5318, Toulouse, France


THOMAS L. DELWORTH

Geophysical Fluid Dynamics Laboratory, National Oceanic and Atmospheric Administration, Princeton, New Jersey

(Manuscript received 17 May 2018, in final form 5 December 2018)

ABSTRACT

Observed September Arctic sea ice has declined sharply over the satellite era. While most climate models forced by observed external forcing simulate a decline, few show trends matching the observations, suggesting either model deficiencies or significant contributions from internal variability. Using a set of perturbed climate model experiments, we provide evidence that atmospheric teleconnections associated with the Atlantic multidecadal variability (AMV) can drive low-frequency Arctic sea ice fluctuations. Even without AMV-related changes in ocean heat transport, AMV-like surface temperature anomalies lead to adjustments in atmospheric circulation patterns that produce similar Arctic sea ice changes in three different climate models. Positive AMV anomalies induce a decrease in the frequency of winter polar anticyclones, which is reflected both in the sea level pressure as a weakening of the Beaufort Sea high and in the surface temperature as warm anomalies in response to increased low-cloud cover. Positive AMV anomalies are also shown to favor an increased prevalence of an Arctic dipole-like sea level pressure pattern in late winter/early spring. The resulting anomalous winds drive anomalous ice motions (dynamic effect). Combined with the reduced winter sea ice formation (thermodynamic effect), the Arctic sea ice becomes thinner, younger, and more prone to melt in summer. Following a phase shift to positive AMV, the resulting atmospheric teleconnections can lead to a decadal ice thinning trend in the Arctic Ocean on the order of 8%–16% of the reconstructed long-term trend, and a decadal trend (decline) in September Arctic sea ice area of up to 21% of the observed long-term trend.

 Denotes content that is immediately available upon publication as open access.

Corresponding author: Frederic S. Castruccio, fredc@ucar.edu

1. Introduction

Arctic sea ice variations are an important indicator of changes in the climate system. Satellite observations reveal a substantial decline in September Arctic sea ice

DOI: 10.1175/JCLI-D-18-0307.1

© 2019 American Meteorological Society. For information regarding reuse of this content and general copyright information, consult the [AMS Copyright Policy \(www.ametsoc.org/PUBSReuseLicenses\)](https://www.ametsoc.org/PUBSReuseLicenses).

extent since the late 1970s. Most climate model simulations forced by the past evolution of external forcing underestimate this decline (Day et al. 2012; Stroeve et al. 2012), and its significant acceleration since the late 1990s (Comiso et al. 2008; Ogi and Rigor 2013) is mostly not captured (Rampal et al. 2011). This suggests a strong role for natural variability in Arctic climate (Stroeve et al. 2007; Swart et al. 2015; Ding et al. 2017) provided that the simulated sensitivity of the Arctic sea ice to the external radiative forcings is approximately correct. Studies using climate models estimate that 50%–60% of recent Arctic sea ice changes are attributable to anthropogenic global warming, with the remainder resulting from internal variability in the climate system (Kay et al. 2011; Stroeve et al. 2012). Therefore, accurate projections of future Arctic sea ice conditions require an understanding both of the role of externally forced trends in Arctic sea ice decline and of the nature and magnitude of internal variability of Arctic sea ice.

Previous studies have investigated possible drivers of Arctic sea ice variability and identified various physical processes that might be important. Such processes include the atmospheric thermodynamic effect on ice melt (Polyakov et al. 2012), atmospheric dynamic forcing on ice drift (Vihma et al. 2012), northward ocean heat transport in the Atlantic basin (Mahajan et al. 2011), Pacific water inflow (Zhang 2015), and the Arctic amplification of climate warming (Screen and Simmonds 2010) associated with the ice-albedo, water vapor, and cloud radiative feedbacks (Soden et al. 2008). Döscher et al. (2014) provide a comprehensive review of the various mechanisms driving Arctic sea ice change and decline. Recently, several studies also emphasized the importance of synoptic weather activity over the Arctic to explain sea ice variability. For example, Screen et al. (2011) examined the role of mean cyclone activity on Arctic sea ice variability in terms of sea ice motion and extent. They found that during years of large September sea ice loss there were fewer storms over the central Arctic Ocean in late spring and early summer. Another example is the recent study by Wernli and Papritz (2018) that emphasizes the important role of summer Arctic anticyclones in generating seasonal atmospheric circulation anomalies, which contribute to enhanced summertime sea ice melt. Their analysis shows a relatively high correlation between the frequency of summer Arctic anticyclones and the summertime sea ice loss and highlights the fundamental role played by extratropical cyclones in the formation of Arctic anticyclones.

Earlier works also indicated that interannual Arctic sea ice variability is linked to decadal shifts in dominant patterns of atmospheric circulation (e.g., Proshutinsky and Johnson 1997). On interannual time scales, the

dominant cause of atmospheric variability in the Arctic is the Arctic Oscillation (AO), reflecting the strength of the polar vortex (Thompson and Wallace 1998). The AO and the closely related North Atlantic Oscillation (NAO) primarily affect sea ice through changes in winds and ice drift (e.g., Rigor et al. 2002; Inoue and Kikuchi 2007; Stroeve et al. 2011). The positive AO played a role in the Arctic sea ice decline before the late 1990s (Rigor et al. 2002). However, the recent more neutral AO may not be a key driver for later sea ice changes (Maslanik et al. 2007). Other patterns of atmospheric variability, such as the Arctic dipole (AD) (Wu et al. 2006) or the Pacific–North American pattern (PNA) (L’Heureux et al. 2008), may play a more important role.

In contrast, the influence on sea ice of slow modes of variability like the Atlantic multidecadal variability (AMV) is less known (Guemas et al. 2016), largely because of the lack of reliable sea ice data prior to the satellite era. Observational and modeling evidence suggests that AMV is associated with, and possibly the driver of, marked climate anomalies over many areas of the globe (e.g., Sutton and Hodson 2005; Knight et al. 2006; Kavvada et al. 2013). Using multicentury proxy records of Arctic sea ice, Miles et al. (2014) have established a signal of multidecadal fluctuations in sea ice extent that may be related to the AMV. Century-scale temperature measurements show the Arctic surface air temperature variability to be significantly associated with AMV (Johannessen et al. 2016). Recently, Yu et al. (2017) found in their global analysis that the leading mode of sea ice concentration variability is positively correlated with AMV and negatively correlated with the Pacific decadal oscillation (PDO) in observations and reanalysis. According to their analysis, which is constrained by the relatively short sea ice cover record, AMV and the PDO appear to drive anomalous surface air temperature and wind in the two polar regions that drive opposite sea ice concentration changes (a decreasing trend in Arctic sea ice concentration as opposed to the generally increasing trend in Antarctic sea ice concentration). Modeling experiments have also suggested that sea ice extent in the Atlantic sector of the Arctic is influenced by the AMV (Mahajan et al. 2011; Day et al. 2012; Zhang 2015; Delworth and Zeng 2016) through the Atlantic meridional overturning circulation (AMOC). All these results suggest that the faster-than-projected decrease in Arctic sea ice since the late 1990s could be partially attributed to the concurrent warm phase of the AMV and cold phase of the PDO. For instance, Day et al. (2012) attribute 5%–30% of the decline in the September sea ice extent during the satellite era (1979–2010) to AMV-related variability.

In this study, we present model-based evidence that the AMV influences Arctic sea ice via atmospheric

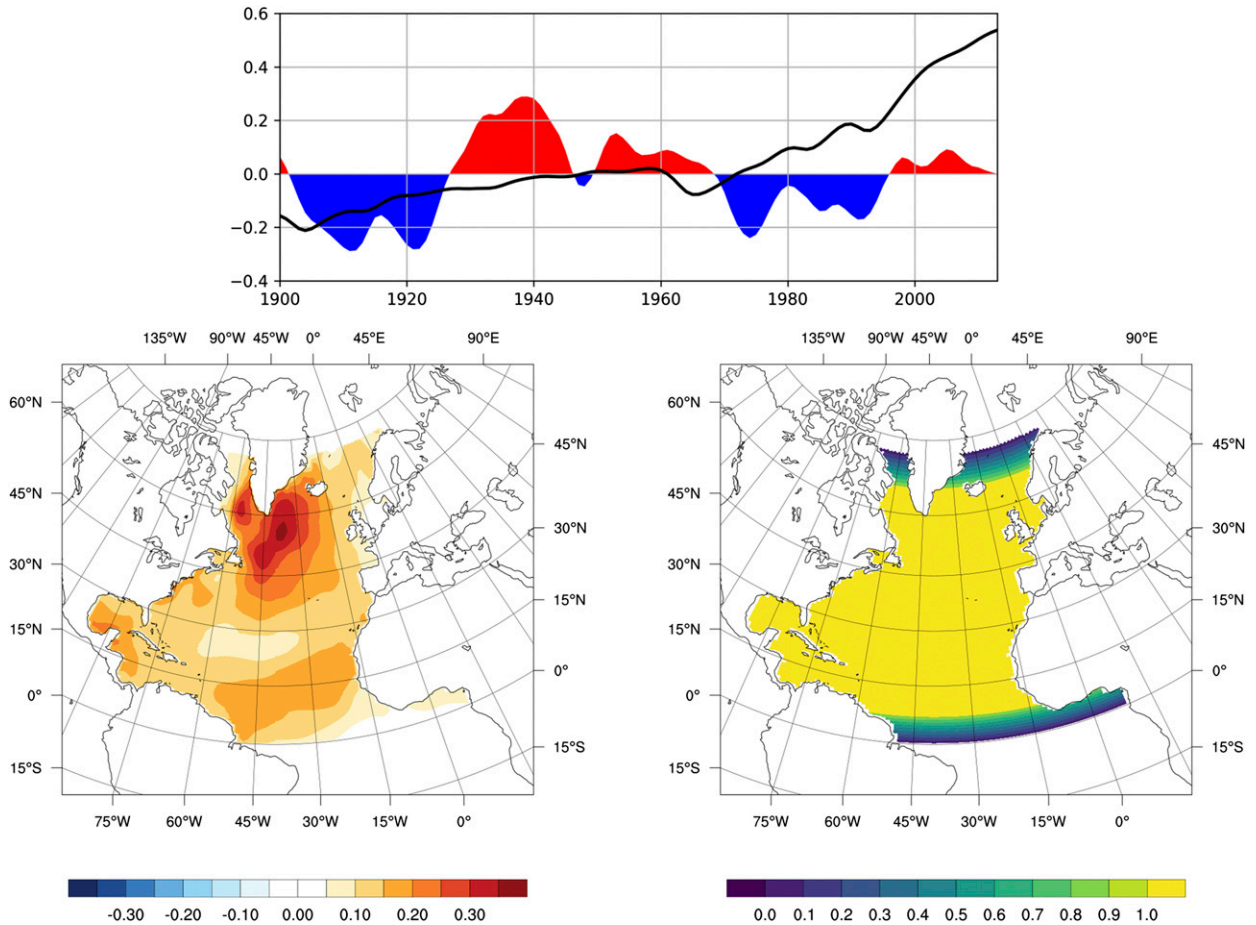


FIG. 1. (top) Internal (red and blue) vs external (black) components of the observed North Atlantic SST decadal variability following Ting et al.'s (2009) definition. (bottom left) Regression map of the observed annual-mean SST (ERSSTv3; Smith et al. 2008) on the internal component of the AMV index (unit is $^{\circ}\text{C}$ per index standard deviation). The regression is shown only over the North Atlantic region (i.e., where the SST restoring is performed in the experiments). (bottom right) Mask used for the SST restoring. Values of 1 and 0 indicate full and no restoring regions, respectively.

teleconnections in addition to its influence via oceanic circulation changes. Our results are based on a set of large ensemble idealized experiments using three state-of-the-art global coupled climate models in which North Atlantic sea surface temperatures (SSTs) are restored to a time-independent spatial pattern corresponding to an estimate of the internal component of the observed AMV anomaly. We argue that the AMV can contribute a substantial fraction of the low-frequency variability of the Arctic sea ice, specifically through atmospheric pathways. Additionally, we show that the atmosphere-driven changes in sea ice linked to AMV are more pan-Arctic than the response of the sea ice to AMV-related oceanic sources of changes described in previous studies. It is thus suggested that the AMV could give rise to predictive skill in the low-frequency modulation of the rate of decline in Arctic sea ice in the Pacific sector, in

addition to the predictive skill linked to the Atlantic Ocean heat transport found in previous studies.

2. Methodology and datasets

To gain insight into the atmospheric teleconnections associated with the AMV and their impacts on the Arctic sea ice, we perform idealized experiments using three climate models in which North Atlantic SSTs are restored to a time-independent spatial pattern corresponding to an estimate of the internal component of the observed AMV anomaly [Fig. 1; see also Ruprich-Robert et al. (2017, hereafter RR17) for more details]. The internal component of the AMV is separated from the externally forced signal, following the approach proposed by Ting et al. (2009). The models are the Community Earth System Model version 1 [CESM1; the

same model version as used in the CESM Large Ensemble simulations described in [Kay et al. \(2015\)](#)], the Geophysical Fluid Dynamics Laboratory (GFDL) Climate Model version 2.1 (CM2.1; [Delworth et al. 2006](#)), and the GFDL Forecast-Oriented Low Ocean Resolution model (FLOR; [Vecchi et al. 2014](#)). All three models use nominal 1° horizontal resolution in their ocean components, but employ different atmospheric resolutions (i.e., 2° in CM2.1, 1° in CESM1, and 0.5° in FLOR). Because we aim to assess the effects of internal variability, all experiments use preindustrial conditions in which external forcings are kept fixed at levels corresponding to either calendar year 1850 (CESM1) or 1860 (FLOR and CM2.1). In all three models, the restoring is fully applied between 8° and 65°N in the North Atlantic, linearly diminishing to zero within 8° buffer zones at the northern and southern boundaries, so that the constrained region is confined between the equator and 73°N ([Fig. 1](#)). Outside of this region, the models evolve freely, allowing a full response of the climate system to the AMV-related SST anomalies. To obtain reliable estimates of the AMV impacts, we perform large ensemble simulations with 30, 50, and 100 members for CESM1, FLOR, and CM2.1, respectively.

For CESM1, SST anomalies corresponding to one standard deviation of the AMV index ([Fig. 1](#)) are added to or subtracted from the models daily climatological SST over the North Atlantic region for the positive (AMV+) or negative (AMV-) AMV experiments, respectively. The restoring time scale is 5 days over 10 m. The CM2.1 and FLOR simulations use a slightly modified protocol to reduce the drift in the ocean component over the North Atlantic subpolar gyre (SPG) seen in these models. As discussed in the supplementary material of [RR17](#), using just the SST restoring in CM2.1 leads to drift in AMOC and ocean heat content over the North Atlantic subpolar gyre that are strong enough to counteract the imposed temperature anomalies over the western SPG, resulting in an anomaly of the opposite sign.¹ Consequently, a “drift-corrected” protocol was introduced for the GFDL models to maintain stable SST anomalies in the SPG during the simulations. Specifically, in the CM2.1 and FLOR experiments, the North Atlantic SSTs are restored to anomalies corresponding to ± 1.5 standard deviation of the observed AMV pattern using a 15-day restoring time scale over 10 m. Along with the SST restoring, the sea surface salinity is also restored to values that counterbalance the surface density anomalies generated by the SST restoring. Given

¹ Although detectable, the drift in CESM1 is much weaker than in CM2.1.

that this slight deviation in the protocol does not result in significant differences in its solutions from those obtained with the original protocol with CM2.1 as demonstrated in the supplementary material of [RR17](#) (see also [Fig. 2](#)), we believe that the comparisons of the responses to the AMV forcing between all three coupled models are meaningful, despite the slightly modified protocol in CM2.1 and FLOR.

Different initialization procedures are followed for CESM1 and for CM2.1 and FLOR. For CESM1, the ensemble members are initialized using a combination of macro- and microperturbations, following [Hawkins et al. \(2016\)](#). First, three different ocean states (macro) are selected from the CESM Large Ensemble preindustrial control simulation as ocean initial conditions. Then, to create a 10-member micro ensemble set for each of these chosen ocean states, the corresponding atmospheric states from the same preindustrial control simulation are perturbed at round-off level in the potential temperature field. For CM2.1 and FLOR, each ensemble member is initialized from an existing preindustrial control simulation, 5 years apart from each other. The model simulations are integrated for a period of 10 years which is long enough for atmospheric teleconnections to arise, yet short enough to limit oceanic drift in the North Atlantic resulting from dynamical adjustments of the ocean at depth to the imposed SST perturbations.

As alluded to above, oceanic sources of variability have been shown to have significant impacts on Arctic sea ice. For example, [Mahajan et al. \(2011\)](#), [Day et al. \(2012\)](#), and [Zhang \(2015\)](#) show that both Arctic sea ice concentration and thickness are negatively correlated with AMOC and Atlantic northward heat transport. [Zhang \(2015\)](#) also shows a negative correlation between Pacific heat transport and Arctic sea ice. In contrast, the idealized experiments used in the present study focus on the impacts of the AMV via atmospheric teleconnections.

3. Arctic sea ice response to AMV-like SST perturbations

[RR17](#) has shown, using the same set of idealized experiments (minus the FLOR ensemble), that the AMV impacts are not just confined to the North Atlantic region. The models simulate teleconnections over the entire globe that are remarkably similar across all models. Many of the simulated impacts are in agreement with the observed impacts such as the teleconnection between the AMV and Sahel rainfall (e.g., [Zhang and Delworth 2006](#)). [RR17](#) also demonstrated that one of the most prominent and robust features in both CESM1

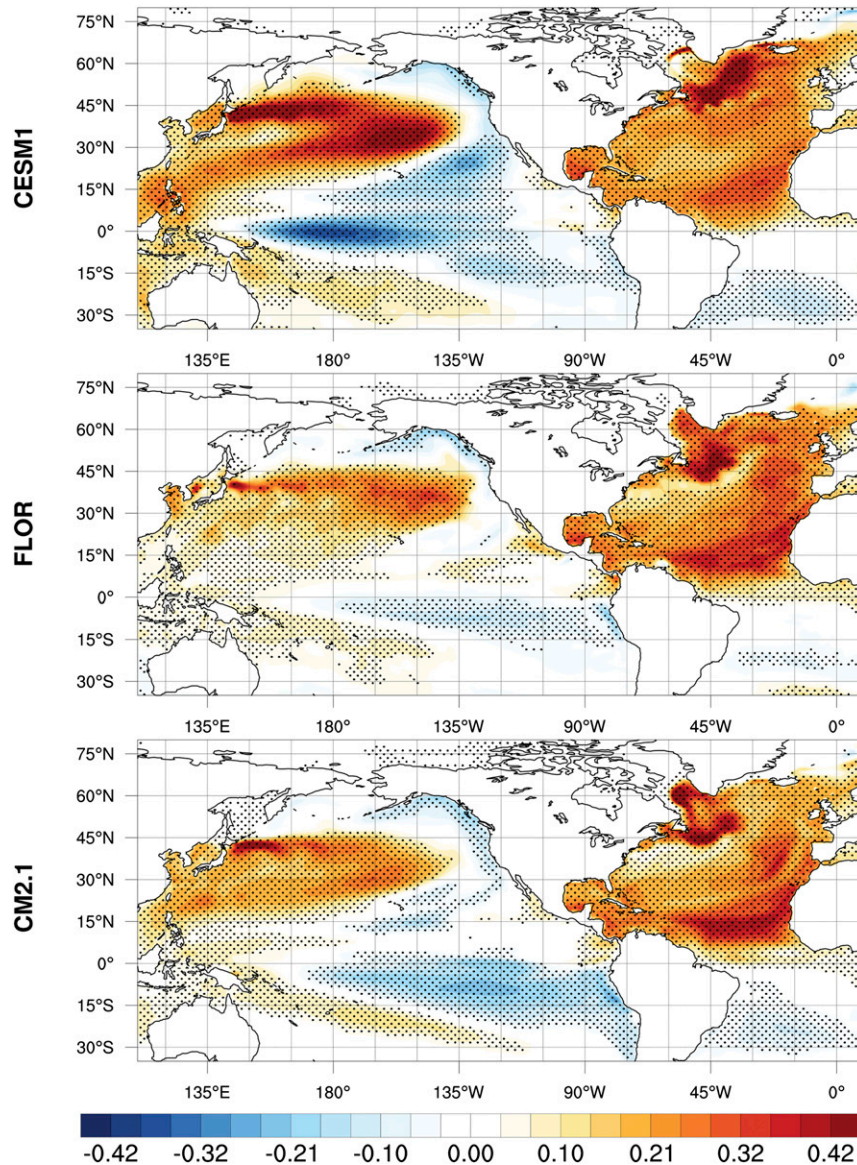


FIG. 2. Differences in 10-yr winter (DJFM) average SST ($^{\circ}\text{C}$) between the AMV+ and AMV- ensemble simulations for (top) CESM1, (middle) FLOR, and (bottom) CM2.1. Stippling indicates regions that are significant above the 95% confidence level based on a two-sided Student's t test.

and CM2.1 is the presence of an interdecadal Pacific oscillation (IPO)-like pattern in its negative phase in response to the AMV warming, similar to the findings of Dong et al. (2006) and Zhang and Delworth (2007). The FLOR simulations, which use the slightly modified protocol described in section 2 and are not discussed in RR17, show the same negative IPO-like pattern (Fig. 2). Figure 2 also illustrates the limited impact of the modified protocol outside of the North Atlantic basin: for CM2.1, in which we have employed both the modified and original protocols, the SST responses to the AMV

forcing are nearly identical in both protocols (cf. Figs. 2 and 4 of RR17).

In the present study, we find in the Arctic basin similarly robust responses to the imposed AMV anomalies in all three models. Differences in winter [December–March (DJFM)] ice thickness between the AMV+ and AMV- ensemble simulations show consistently thinner sea ice during the positive phase of the AMV (Fig. 3). The largest signals are found in the Eastern Siberian Sea and Chukchi Sea with reduced thicknesses of $>10\%$ of the mean seasonal ice pack thickness averaged over the

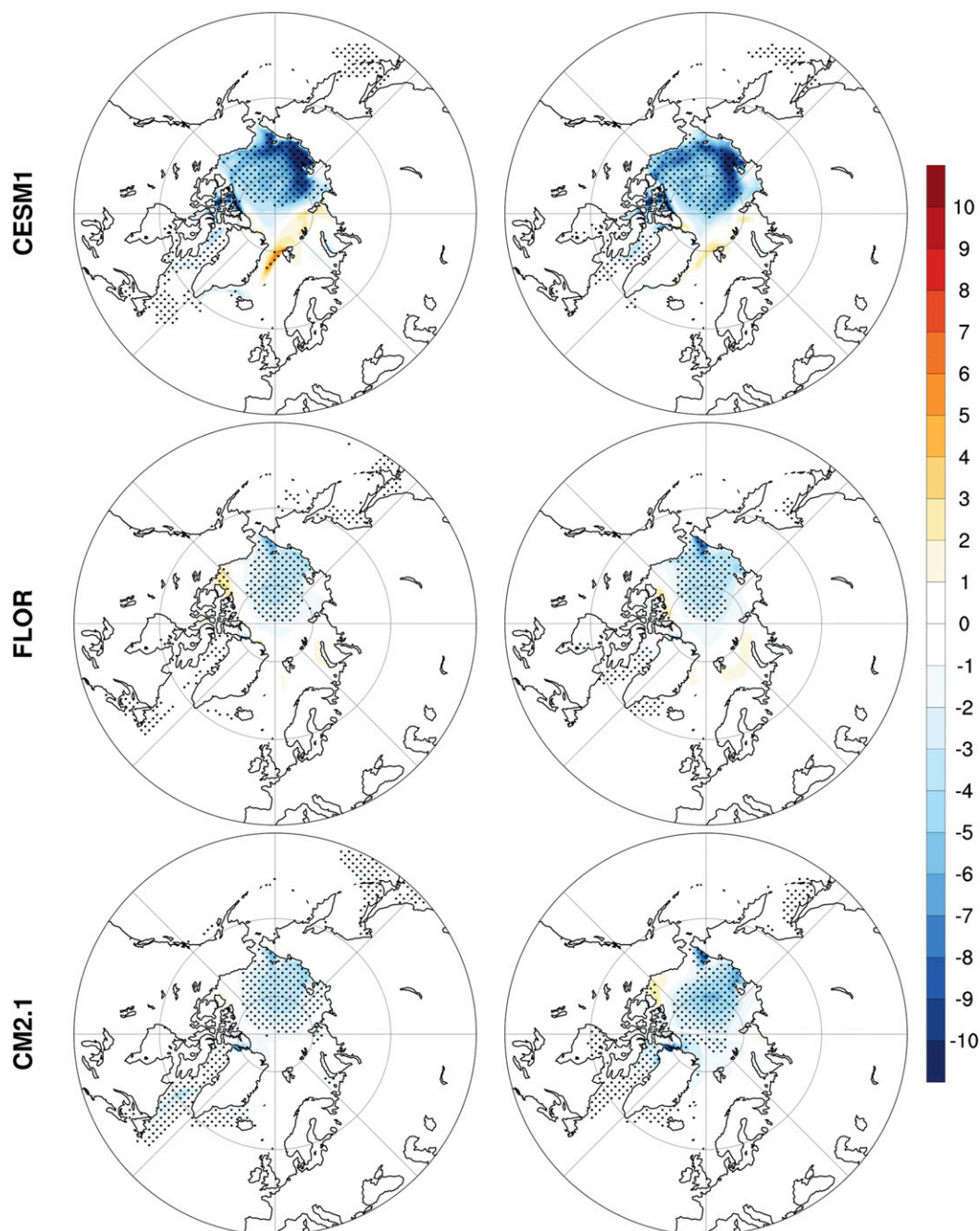


FIG. 3. Differences in 10-yr (left) winter (DJFM) and (right) summer (JJAS) average sea ice thickness between the AMV+ and AMV- ensemble simulations for (top) CESM1, (middle) FLOR, and (bottom) CM2.1. The differences are expressed in percent of the mean seasonal ice pack thickness averaged over the Arctic Ocean. Stippling indicates regions that are significant above the 95% confidence level based on a two-sided Student's t test.

Arctic Ocean in CESM1, corresponding to a >30 -cm reduction in thickness (not shown), with a same-signed response extending across most of the Arctic basin. The pattern is quite similar between the models although the magnitude of the response is stronger in CESM1 than in FLOR and CM2.1 (Fig. 3); this difference will be

discussed in section 5. There is a winter reduction in ice concentration along the ice edge in the Labrador, Irminger, and Barents Seas in CM2.1 and CESM1 (Fig. 4). In the Pacific sector, all three models simulate less extensive winter sea ice in the Sea of Okhotsk (Fig. 4). The winter retreat of the ice edge in those regions

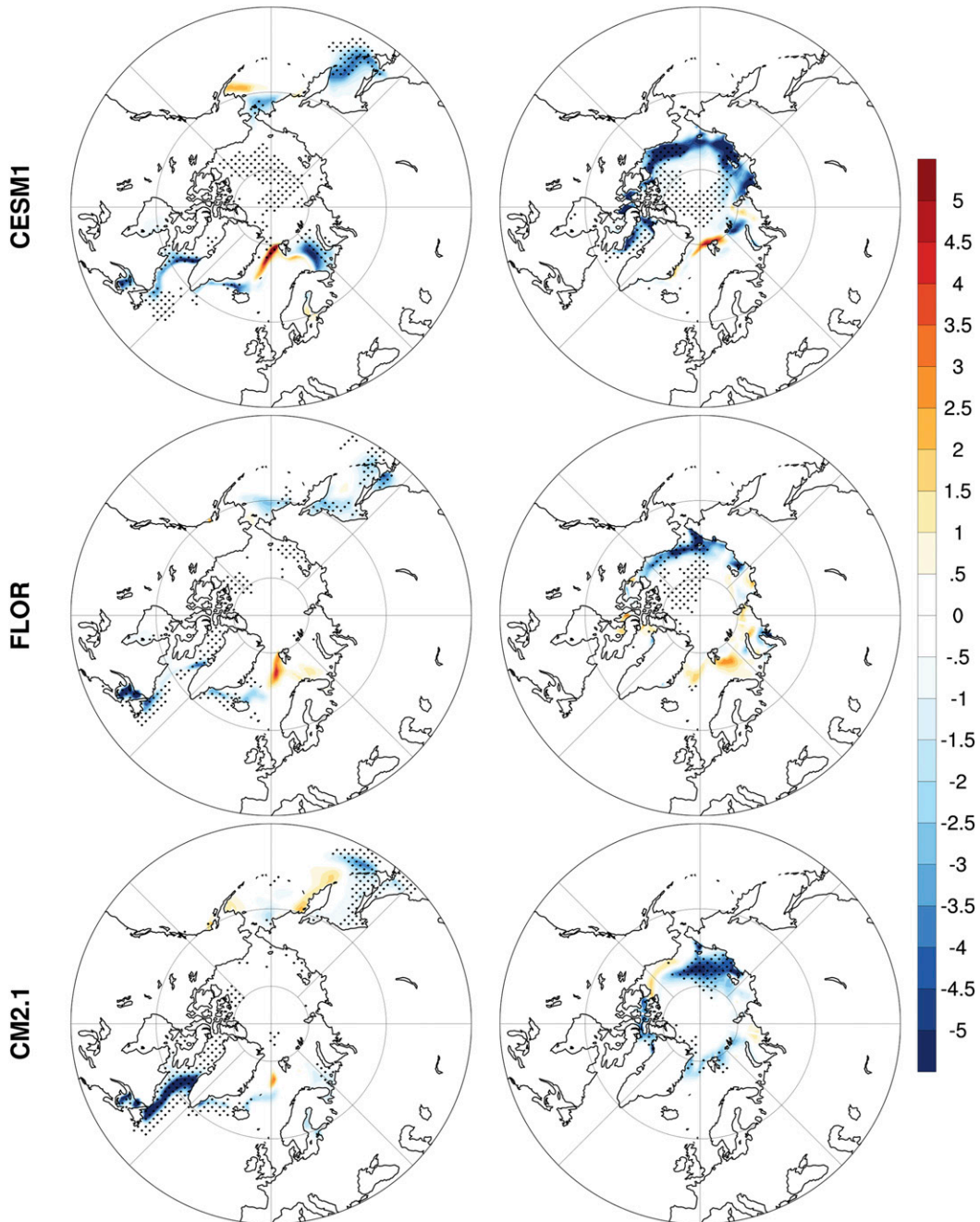


FIG. 4. Differences in 10-yr (left) winter (DJFM; %) and (right) September (%) average sea ice concentration between the AMV+ and AMV- ensemble simulations for (top) CESM1, (middle) FLOR, and (bottom) CM2.1. Stippling indicates regions that are significant above the 95% confidence level based on a two-sided Student's t test.

is presumably due to the warmer SSTs associated with the AMV+/IPO- pattern (Fig. 2). All three models also show a small increase in sea ice concentration just south of the Fram Strait, which is consistent with an increased winter ice export (discussed in the next section). The differences in ice thickness between the AMV+ and

AMV- ensemble simulations depicted in Fig. 3 tend to grow with time as shown in Fig. 5.

The summer [June–September (JJAS)] ice thickness response resembles the winter response (Fig. 3). Reductions in summer ice concentration exceed 5% around the ice edge at the end of the melt season

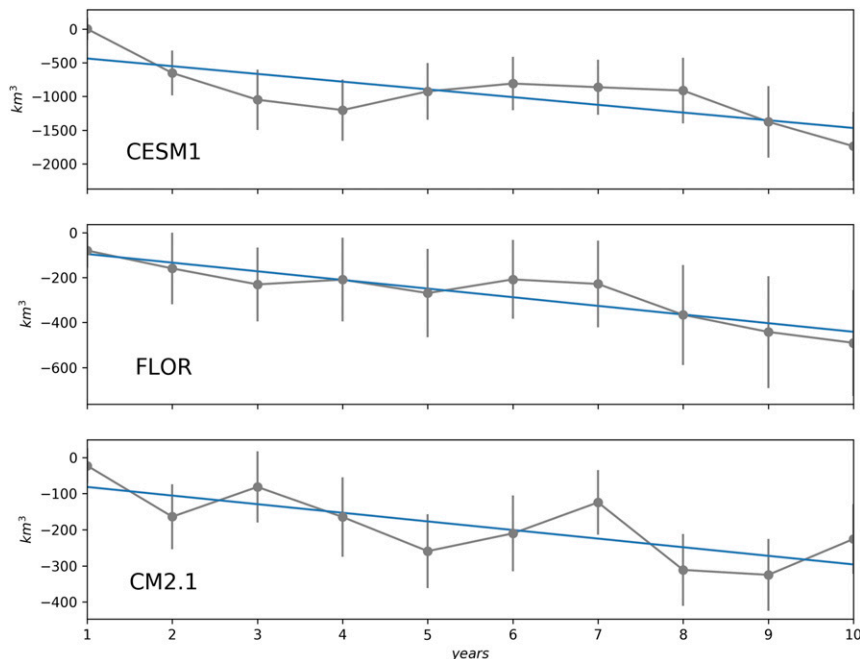


FIG. 5. Differences in yearly Arctic Ocean basin sea ice volume between the AMV+ and AMV- ensemble simulations for (top) CESM1, (middle) FLOR, and (bottom) CM2.1. The linear trend is shown in blue for each model.

(September). Similar to Arctic sea ice volume, we find a negative trend in September Arctic sea ice area (Fig. 6). Such a link between ice thickness and summer ice area is well documented. Blanchard-Wrigglesworth et al. (2011), for example, explore this link in the context of seasonal Arctic sea ice prediction, showing how Arctic ice thickness can serve as a memory reservoir to carry ice area anomalies through the winter, and hence be used as a predictor of the September ice area minimum. Blanchard-Wrigglesworth et al. (2011) also describe melt-to-growth season reemergence patterns, where sea ice area anomalies during the melt season are reflected in the following growth season. In this case SST anomalies in the vicinity of the sea ice edge provide the memory. However, this SST persistence mechanism cannot explain the trend in the central Arctic under the multiyear ice seen in our experiments, because SST anomalies cannot persist in winter past freeze-up. Chevallier and Salas-Méliea (2012) and Day et al. (2014) also show that an accurate knowledge of the sea ice thickness field is necessary to forecast summer ice extent. In our simulations, the thinner winter ice cover associated with AMV+ melts and opens up more readily in summer, resulting in reduced ice concentration at the end of the melt season. The changes in ice concentration are further enhanced by the ice-albedo feedback, which acts to reinforce the initial changes in ice area (Curry et al. 1995). Specifically, a decrease in ice

cover reduces the surface albedo (Fig. 7), leading to greater radiation absorption by the ocean, thus contributing to surface warming (Fig. 7) and further enhancing the melt rate. The enhanced summer warming later delays the fall freeze-up, resulting in negative thickness anomalies that carry the information through the winter to the next melt season.

As detailed in section 2, our experimental protocol was designed to limit dynamical adjustments of the ocean and associated changes in northward oceanic heat transport in order to focus on the atmospheric teleconnections associated with the AMV. We confirmed that changes in northward heat transport from the Atlantic into the Arctic Ocean are negligible in CESM1, and hence cannot be the mechanism behind the simulated changes in Arctic sea ice in our idealized AMV experiments. Defining the Arctic basin as the region north of 68°N between 100° and 243°E and north of 80°N over the Atlantic sector following Holland et al. (2010), we compute the 10-yr annual average northward heat transport by the Atlantic Ocean at 80°N as 1.67 and 1.64 TW in CESM1 for the AMV+ and AMV- experiments, respectively.² These transports are not significantly

²The meridional ocean heat transport was only archived for CESM1, and thus, we limit our oceanic heat transport analysis to this model.

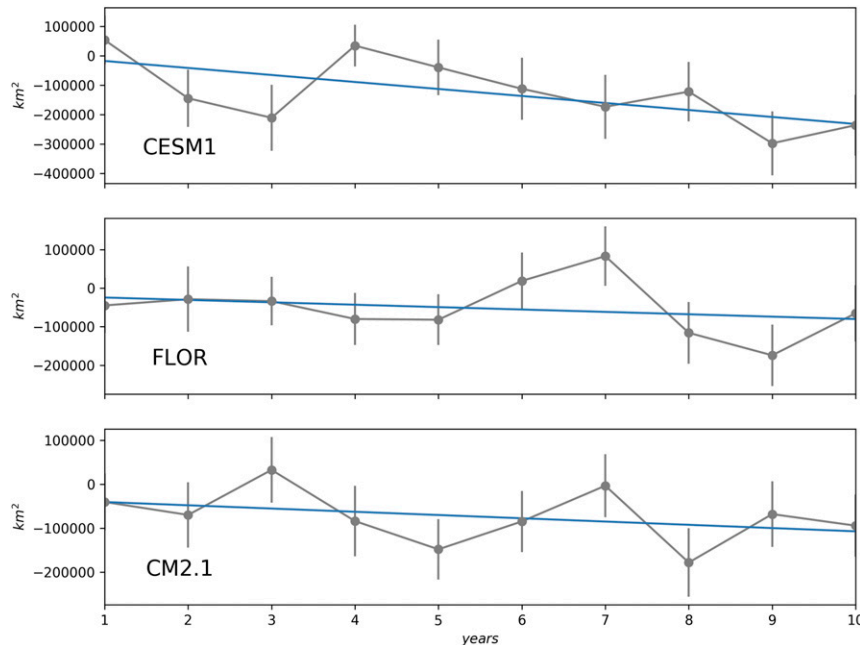


FIG. 6. Differences in September Arctic Ocean basin sea ice area between the AMV+ and AMV– ensemble simulations for (top) CESM1, (middle) FLOR, and (bottom) CM2.1. The linear trend is shown in blue for each model.

different according to a t test. The change in northward heat transport through the Bering Strait between the AMV+ and AMV– experiments is not statistically significant in CESM1, either, with 10-yr annual average transports of 2.90 and 2.87 TW, respectively. Given that the combined increase of the Atlantic and Pacific Ocean heat transports into the Arctic of 0.06 TW during the AMV+ phase can melt only about 6 km^3 of sea ice over a year,³ or about 60 km^3 over 10 years, the simulated ice volume change of over 1500 km^3 after 10 years in CESM1 between the AMV+ and AMV– ensembles (Fig. 5) cannot be attributed to the ocean heat transport change. Therefore, we conclude that the changes in the Arctic that result from atmospheric circulation and/or teleconnections are the primary driver of the simulated changes in Arctic sea ice thickness and concentration.

4. Changes in Arctic atmospheric circulation

RR17 showed that AMV leads to a Pacific response in winter that projects onto the IPO and PNA. In association with the negative PNA pattern, all models simulate a strong weakening of the winter Aleutian low

(Fig. 8). Over the Arctic, all models simulate negative sea level pressure (SLP) anomalies, associated with a weakening of the Beaufort Sea high (BSH; Fig. 8). Serreze and Barrett (2011) have shown that the frequency of anticyclonic surface winds is a good indicator of the strength of the BSH. They found strong positive correlations between SLP and vorticity over the Arctic Ocean, with correlations larger than 0.6 over the Beaufort Sea. In winter, the frequency of anticyclonic events in the BSH region is also negatively correlated with SLP in the Aleutian low region of the North Pacific. To investigate if such relationships exist in our simulations, we examine the winter percentage frequency of negative (anticyclonic) and positive (cyclonic) relative vorticity events between the AMV+ and AMV– ensemble simulations, using daily winds at 850 hPa and focusing only on CESM1 solutions. For a given location, anticyclonic frequency is defined as the percentage of all wintertime events for each AMV+ and AMV– ensemble when the relative vorticity was more negative than the 25th percentile of all negative events for AMV+ and AMV– ensembles combined. Cyclonic percentage frequency is computed the same way using positive vorticity events exceeding the 75th percentile of all positive events. We use the 25th percentile threshold in order to retain only the strong synoptic events since the strength rather than the overall number of events has been shown to play an important role (e.g., Simmonds

³The energy required to melt a cubic meter of sea ice is $e = \rho_i \Lambda_F$, where Λ_F is the latent heat of fusion ($\Lambda_F = 334\,000 \text{ J kg}^{-1}$) and ρ_i is the density of sea ice ($\rho_i = 905 \text{ kg m}^{-3}$).

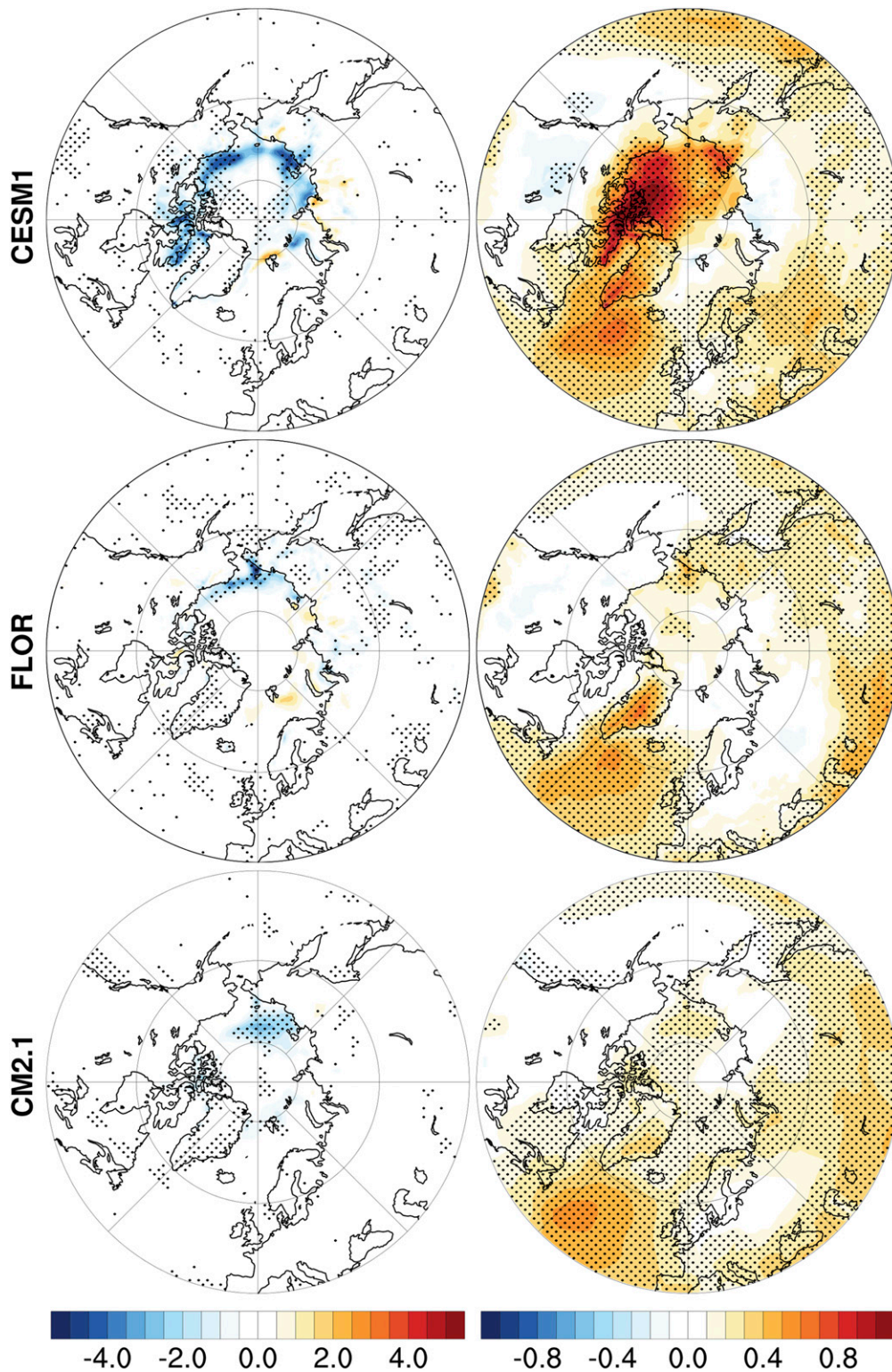


FIG. 7. Differences in 10-yr September average (left) albedo (%) and (right) surface air temperature (°C) between the AMV+ and AMV- ensemble simulations for (top) CESM1, (middle) FLOR, and (bottom) CM2.1. Stippling indicates regions that are significant above the 95% confidence level based on a two-sided Student's *t* test.

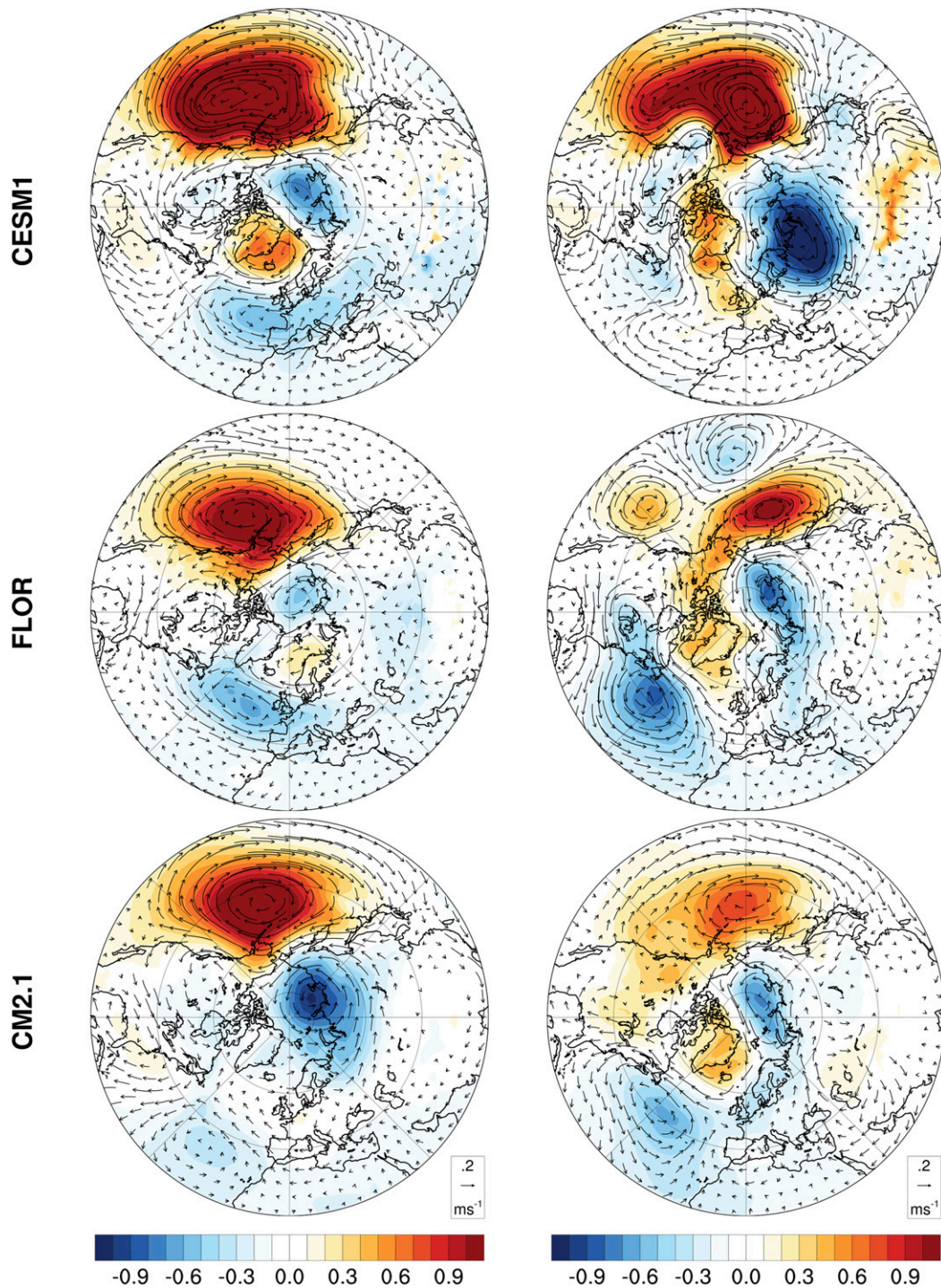


FIG. 8. Differences between the AMV+ and AMV- ensemble simulations in (left) 10-yr winter (DJFM) average SLP (hPa) with the resulting anomalous winds at 850 hPa overlaid and (right) 10-yr average SLP (hPa) with the resulting near-surface anomalous winds overlaid for CESM1 in March, and FLOR and CM2.1 in April. For all columns, results are for (top) CESM1, (middle) FLOR, and (bottom) CM2.1. The reduction in the Beaufort high pressure as well as the dipole response in SLP in late winter (see right panels) are statistically significant in all three models (not shown).

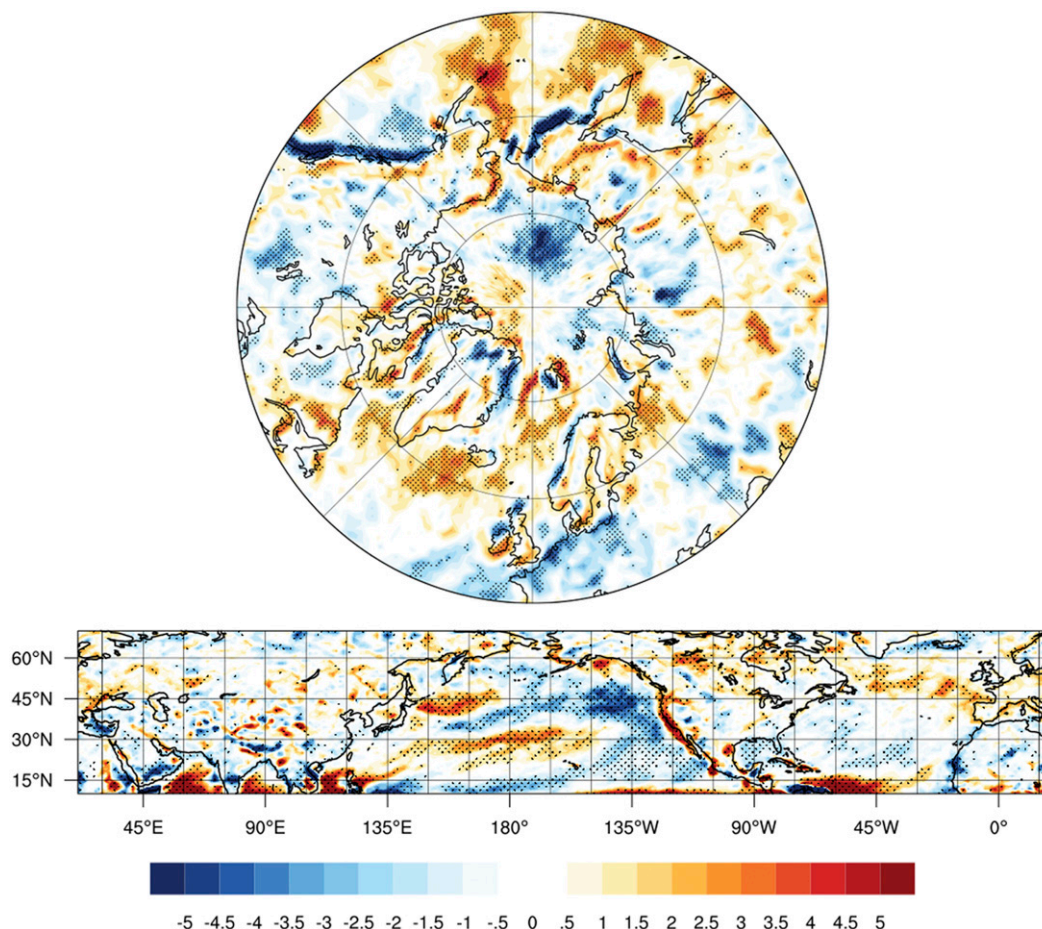


FIG. 9. Differences in percentage frequency of (top) Arctic anticyclonic winds and (bottom) midlatitude cyclonic winds at 850 hPa in winter (DJFM) between the AMV+ and AMV- ensemble simulations for CESM1. Stippling indicates regions that are significant above the 95% confidence level based on a two-sided Student's t test.

and Keay 2009). Figure 9 (top) shows the composite differences of winter percentage frequency of anticyclonic events over the Arctic from CESM1. The model simulates a clear reduction of strong anticyclonic events over the Arctic in winter. The region with reduced anticyclone frequency is collocated with the area where the model also simulates negative SLP anomalies, in agreement with Serreze and Barrett (2011) indicating that frequency of anticyclonic events is positively correlated with the strength of the BSH. Following the work by Wernli and Papritz (2018) showing that air masses contributing to Arctic anticyclones are injected from midlatitudes into the Arctic in association with extratropical cyclones, we also show the composite difference distributions of winter percentage frequency of cyclonic events between AMV+ and AMV- ensembles over the midlatitude regions (Fig. 9, bottom panel). We again find a reduction in cyclone frequency in the northwest Pacific around 40°N associated with the

poleward shift of the storm track (RR17). Such a relationship between the meridional position of the Pacific storm track and the phase of the PDO in winter has been previously described by Sung et al. (2014). East of the date line, we also find a large reduction in cyclone activity in the North Pacific (Fig. 9) in association with the strong weakening of the winter Aleutian low (Fig. 8). The imprint of the more zonal North Pacific SST front associated with the PDO- (AMV+) phase on the atmospheric surface circulation could also play a role by creating a region of diminished cyclonic potential vorticity and cyclogenesis in the Gulf of Alaska (Pickart et al. 2009). Consistent with the findings of Wernli and Papritz (2018), we contend that the reduced anticyclone frequency simulated by CESM1 in the Arctic is at least partially attributable to the reduced frequency of cyclonic storm events in the extratropical North Pacific.

Along with the reduced frequency of anticyclones in the Arctic (and increased frequency of cyclones; not

shown), CESM1 also simulates an enhancement of the winter low cloud cover over the Arctic Ocean (Fig. 10, top). Arctic low clouds (cloud-top height < 3 km) have a large influence on the Arctic surface energy budget (Kay and Gettelman 2009). For example, based on observations from the Surface Heat Budget of the Arctic Ocean (SHEBA) program (Uttal et al. 2002), Shupe and Intrieri (2004) estimate that the net cloud radiative forcing at the Arctic surface is about 20 W m^{-2} despite nearly zero incoming solar radiation during the dark winter months. This is due to the strong longwave radiative effect of Arctic clouds, which absorb and re-emit longwave radiation from Earth's surface. As a result, the surface temperature in the Arctic during winter is strongly affected by cloud cover. While Arctic clouds have a large impact on radiative fluxes and are a major factor of the Arctic climate, numerous and complex interactions between various physical processes have made it difficult to understand how clouds form and evolve in time (Morrison et al. 2012). Despite the complexity of the system, the observations support the existence of two distinct, persistent states corresponding to radiatively clear and opaquely cloudy conditions [see Fig. 4 in Morrison et al. (2012)]. The specific meteorological conditions as well as the large-scale environment favoring each state are uncertain but Fig. 4 in Morrison et al. (2012) shows that radiatively clear conditions tend to be associated with higher sea level pressure whereas cloudy conditions correspond to lower sea level pressure. For this reason, the decrease in synoptic anticyclonic frequency and the associated decrease in seasonal sea level pressure simulated by CESM1 is most likely favoring opaquely cloudy conditions, and can explain the enhancement of the winter low cloud cover seen in this model (Fig. 10, top). While the atmospheric northward heat transport into the Arctic is not significantly affected by the AMV phase in CESM1,⁴ the model simulates a weak increase of northward humidity transport into the Arctic. Availability of this additional moisture also likely favors cloud formation. Along with the enhanced winter cloud cover, CESM1 simulates winter surface warming in the Arctic during the AMV+ phase (Fig. 10, bottom). Because the net surface heat flux over the Arctic Ocean and the convergence of heat into the Arctic basin do not change between the AMV+ and AMV- simulations appreciably, the winter warming simulated by CESM1 is most likely associated with

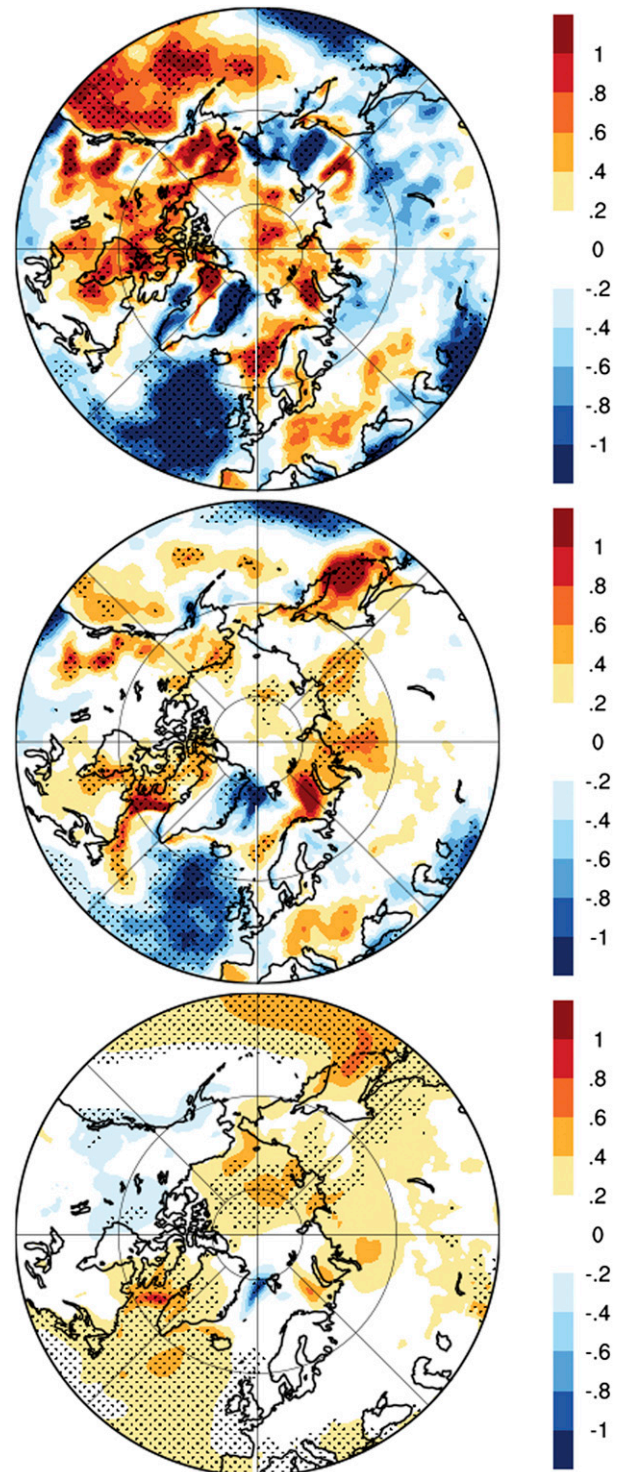


FIG. 10. Differences in 10-yr winter (DJFM) (top) average low cloud cover (%), (middle) longwave radiative cloud forcing at the surface (W m^{-2}), and (bottom) temperature at the surface ($^{\circ}\text{C}$) between the AMV+ and AMV- ensemble simulations for CESM1. Stippling indicates regions that are significant above the 95% confidence level based on a two-sided Student's t test.

⁴The 10-yr annual mean northward atmospheric heat transport at 70°N is 1.605 PW on average for the AMV+ ensemble, and 1.611 PW for the AMV- ensemble for CESM1. This difference of 6 TW is not statistically significant according to a t test.

the simulated increased downwelling longwave radiation at surface (not shown) as a response to the simulated increased cloudiness over the Arctic Ocean. To further support this proposed causal link that surface warming is caused by the increase in low clouds cover, we have computed the differences in 10-yr winter (DJFM) average longwave radiative cloud forcing at the surface between the AMV+ and AMV- phases (Fig. 10, middle). The longwave radiative cloud forcing is obtained as the difference between the all-sky net surface longwave flux and the clear-sky net surface longwave flux. The fluxes are defined as positive downward, meaning that a positive cloud forcing indicates that clouds increase the amount of radiation at the surface (i.e., a warming effect), whereas a negative cloud forcing indicates surface cooling. The positive longwave radiative cloud forcing anomalies simulated by CESM1 over the central Arctic during the AMV+ phase (Fig. 10, middle) are consistent with the increased cloud cover (Fig. 10, top), suggesting that surface warming (Fig. 10, bottom) is indeed caused by the enhancement of the winter low cloud cover in this model.

In late winter/early spring, an anomalous dipole pattern in SLP exists in all three models (Fig. 8, right panels), with a high SLP anomaly on the North American side of the Arctic and a low SLP anomaly on the Eurasian side during AMV+. The pattern of SLP anomalies is robust across all models, but the timing is slightly different: the dipole pattern is more pronounced in March in CESM1, and in April in FLOR and CM2.1. Although the dipole anomaly is short lived in our simulations, it induces enhanced transpolar winds (Fig. 8, right panels), thus making it an important mechanism to drive anomalous sea ice export out of the Arctic basin.

Our idealized experiments thus show that AMV-related atmospheric teleconnections produce consistent changes in Arctic atmospheric circulation in three different climate models that impact the Arctic sea ice pack through both dynamic forcing on ice drift and thermodynamic effects on winter sea ice formation. For the latter, the warm winter surface anomalies associated with increased cloudiness and increased downwelling longwave radiation slow down Arctic sea ice growth in winter. Regarding the former, the wind anomalies associated with SLP anomalies alter the two main components of the wind-driven ice drift pattern in the Arctic: 1) the Beaufort Gyre, a clockwise (anticyclonic) motion of sea ice in the Beaufort Sea, keeping sea ice in the Arctic basin; and 2) the Transpolar Drift Stream (TPDS), a current transporting ice from the Siberian coast toward Fram Strait and into the North Atlantic (Emery et al. 1997; Fig. 8). The anomalous cyclonic winds over the central Arctic in response to the weaker

BSH (Fig. 8, left panels) drive an anomalous cyclonic ice motion (Fig. 11), which tends to push the old multiyear ice out of the central Arctic and into the pathway of the TPDS (Rigor et al. 2002). Sea ice that gets captured in the TPDS generally leaves the Arctic more quickly without enough time to grow and reach thermodynamic equilibrium, thus resulting in a younger and thinner ice pack (e.g., Nghiem et al. 2007; Hansen et al. 2013). All three models show a slight increase in winter (November to April) sea ice export through both the Fram Strait and the passage between Svalbard and Franz Josef Land, coincident with the period (from October to April) when the observed ice export is high, driven by increased ice speed related to winds and ocean currents (Langehaug et al. 2013). The sea ice export increase peaks in March for CESM1 at 5%, and in April for FLOR and CM2.1 at 2% and 3%, respectively. This is consistent with an accelerated TPDS shifted toward the Canadian Archipelago (Fig. 12) in response to the enhanced transpolar wind in late winter/early spring (Fig. 8, right panels) forced by the dipole pattern in SLP. The simulated ice thinning and larger ice export in our idealized AMV experiments are consistent with previous studies that have linked the Fram Strait ice export with the Arctic basin ice thickness at seasonal (Smedsrud et al. 2017) and interannual time scales (Langehaug et al. 2013).

The dipole pattern in SLP also favors late winter offshore winds in the Laptev Sea and adjacent Siberian seas, driving larger than average sea ice export. A recent study by Itkin and Krumpen (2017) that uses both observations and model simulations shows the thinning effect of such late winter offshore winds that open polynyas at the fast ice edge. The new sea ice grown in the polynyas remains thin and melts quickly in summer resulting in early ice retreat and low ice cover in the Laptev Sea and adjacent Siberian seas. Itkin and Krumpen (2017) results show that this preconditioning of the summer sea ice state by the late winter offshore winds and ice export is more important than the winter ice thickness itself.

Together, the anomalous wind-driven ice motions (dynamic effect) and the reduced winter sea ice growth (thermodynamic effect) restructure the Arctic sea ice into a thinner (Fig. 3) and younger (Fig. 13, top) pack that is more prone to melt, resulting in reduced ice extent at the end of the melting season (Fig. 4). The albedo feedback then provides a positive feedback that acts to reinforce the initial changes in ice area. The reductions in ice thickness also lead to a weakening of the ice mechanical strength (Fig. 13, bottom) during AMV+, creating another positive feedback as an ice pack with weaker mechanical strength is more responsive to winds (e.g., Rampal et al. 2009; Kwok et al. 2013).

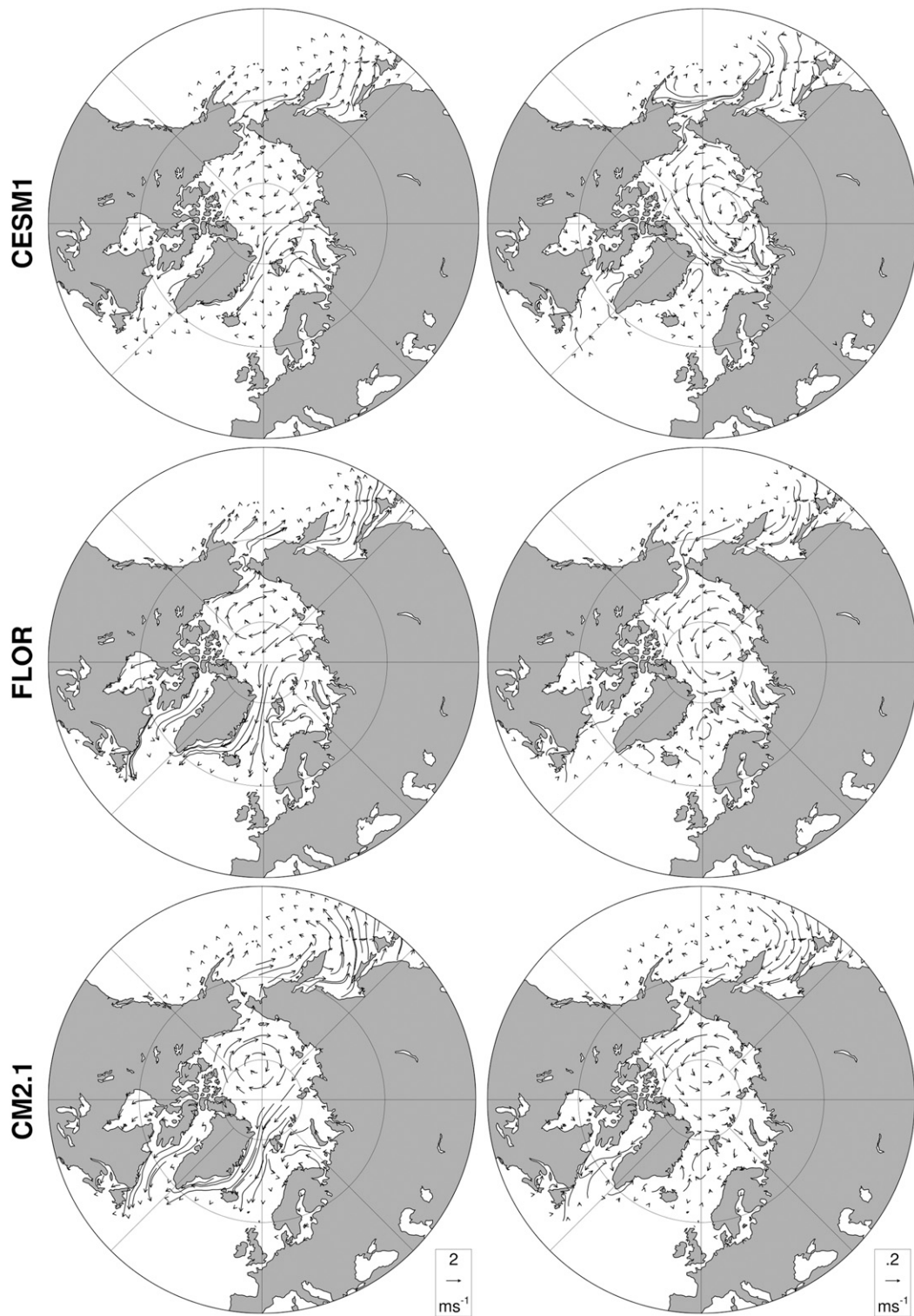


FIG. 11. (left) The 10-yr DJFM average ice motion for the combined AMV+ and AMV- ensembles and (right) the differences between the AMV+ and AMV- ensembles, for (top) CESM1, (middle) FLOR, and (bottom) CM2.1.

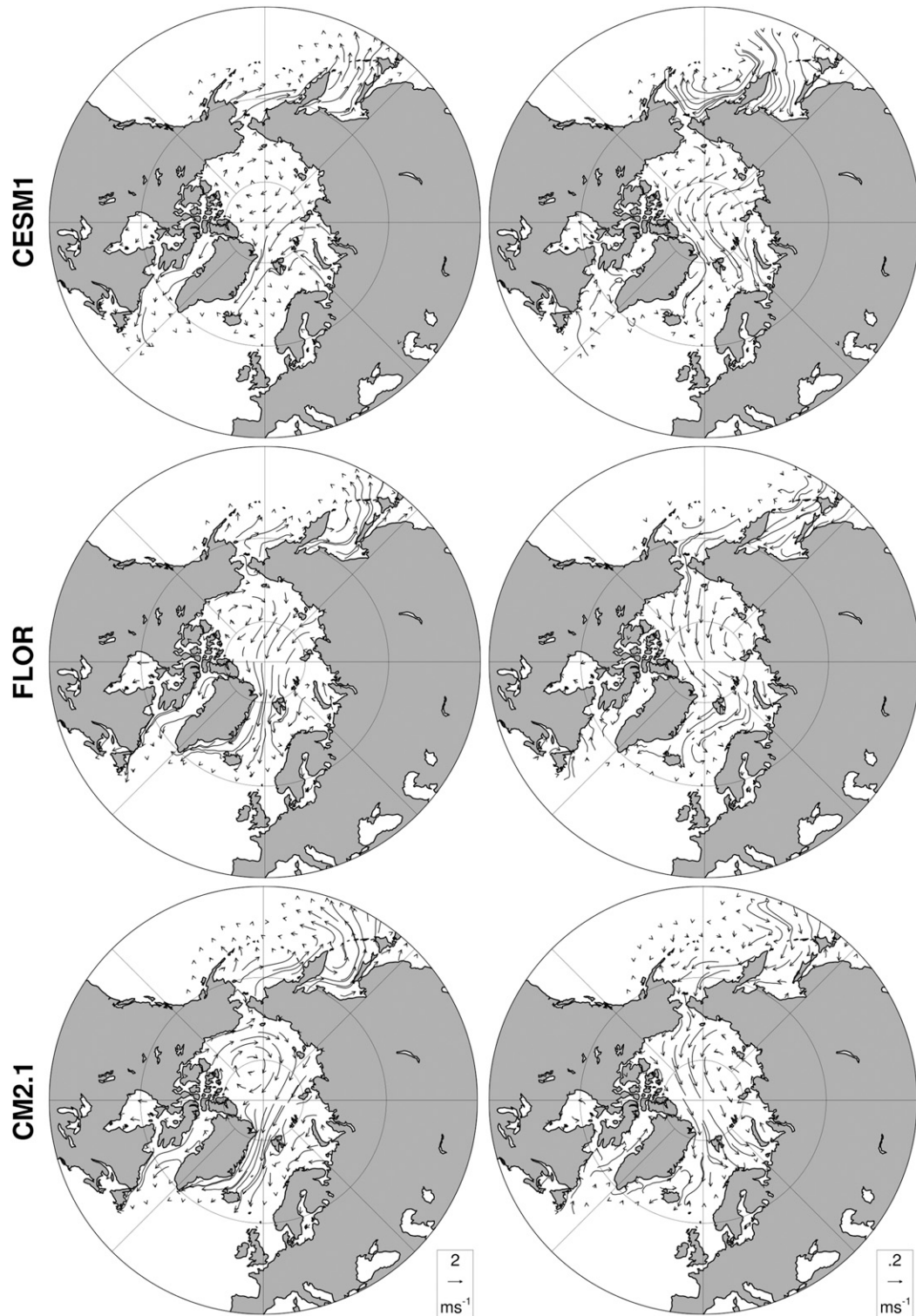


FIG. 12. The 10-yr average ice motion for (top) CESM1 in March, (middle) FLOR in April, and (bottom) CM2.1 in April for (left) the combined AMV+ and AMV- ensembles and (right) the differences between the AMV+ and AMV- ensembles.

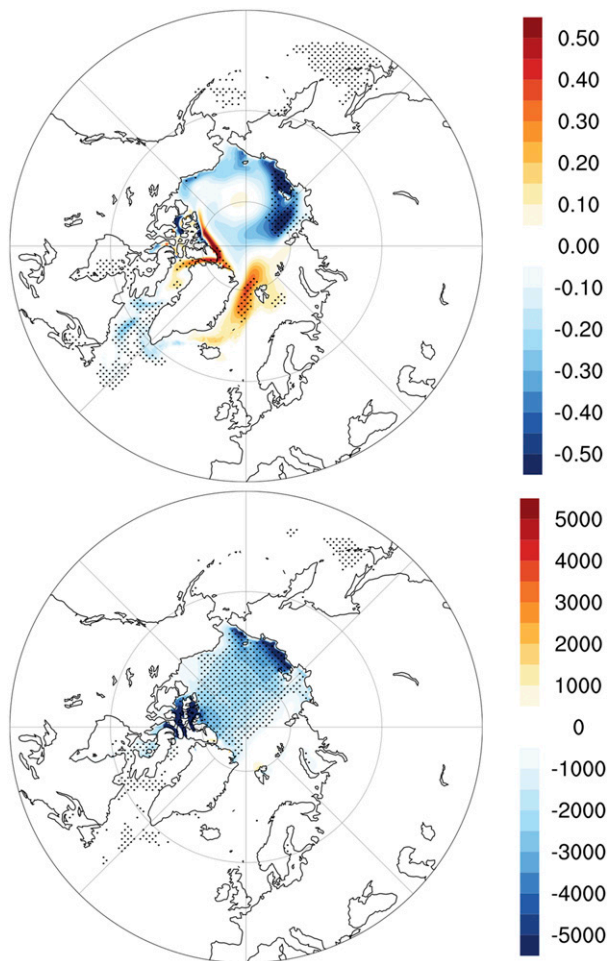


FIG. 13. Difference in 10-yr annual average (top) ice age (yr) and (bottom) ice strength (N m^{-1}) between the AMV+ and AMV- ensemble simulations for CESM1. The ice age and ice strength were not archived for CM2.1 and FLOR. Stippling indicates regions that are significant above the 95% confidence level based on a two-sided Student's t test.

5. Discussion and conclusions

We have analyzed the impacts of the surface signature of the AMV on the Arctic climate using ensembles of idealized experiments with three state-of-the-art coupled climate models in which the North Atlantic SSTs are restored to a time-independent spatial pattern corresponding to an estimate of the internal part of the observed AMV anomaly. Based on our experiments, the AMV warming leads to a positive IPO pattern in the Pacific (see also RR17), leading to a broad Northern Hemisphere extratropical warming. We also identify a negative PNA pattern in the Pacific. In CESM1, we find a reduction of the frequency of midlatitude cyclones. Consistent with Sung et al. (2014), the reduction of the frequency of cyclones around 40°N appears to be

associated with a poleward shift of the storm track in the western Pacific. East of the date line, the strong weakening of the Aleutian low is associated with a reduction of the frequency of cyclones. The more zonal North Pacific front could also play a role in the reduction of the cyclogenesis in the Gulf of Alaska (Pickart et al. 2009). Consistent with the findings of Wernli and Papritz (2018) where Arctic anticyclones have been shown to result from extratropical cyclones, we find a reduction of the frequency of winter Arctic anticyclones in our simulations in association with the decrease in the frequency of midlatitude cyclones. This reduction of the frequency of winter Arctic anticyclones is reflected in the seasonal mean SLP with negative SLP anomalies over the Arctic during the AMV+, in agreement with previous studies showing that the frequency of anticyclonic events is positively correlated with the strength of the BSH. The reduction in synoptic anticyclone frequency and a weakened BSH, in turn, appear to drive an increase in low cloud cover in CESM1, likely through the opaquely cloudy conditions associated with lower SLP as discussed in Morrison et al. (2012). Such enhanced cloudiness during the dark winter months leads to surface warming through cloud radiative forcing. In addition to the weaker BSH and warm surface anomalies in winter, our results reveal an anomalous SLP dipole pattern in late winter/early spring with an anomalous high (low) on the North American (Eurasian) side of the Arctic during the AMV+. Along with a slowdown in winter ice growth associated with warmer surface temperatures, anomalous winds drive ice motion anomalies that result in a thinner sea ice pack in all three climate models. Our results agree with a recent observation-based analysis by Yu et al. (2017) showing that the leading mode of global sea ice concentration variability appears to be positively correlated with the AMV and negatively correlated with the PDO. In our simulations, the anomalous ice motions combined with the thinner Arctic sea ice, which is more prone to melt, lead to less extensive Arctic sea ice at the end of the melting season. The summer ice melt is further enhanced by the ice-albedo feedback, which acts to reinforce the initial changes in ice extent. Another positive feedback comes from the reduction in the sea ice mechanical strength in response to the sea ice thinning, which makes the ice pack more vulnerable to winds.

All three models show a consistent response in Arctic sea ice thickness due to the AMV forcing. However, the magnitudes of the response differ quite substantially between the models. The simulated climatological ice pack is also substantially different between the models. The annual mean ice thickness over the Arctic basin is

3.2, 2.1, and <1 m for CESM1, FLOR, and CM2.1, respectively. CM2.1 is known to simulate extremely thin sea ice (Griffies et al. 2011), partly due to the albedo settings and to a deficiency in the representation of the BSH (Kwok 2011). Bitz and Roe (2004) describe how the growth–thickness relationship defines a feedback process that leads to small equilibrium thickness changes when thin ice is subject to a perturbation, but results in larger equilibrium thickness changes for thicker ice. It is worth noting that this relationship can be modified by sea ice dynamics and feedback effects (Pithan and Mauritsen 2014), but according to Bitz and Roe (2004) the growth–thickness feedback dominates, and therefore could explain the differences in the magnitude of the thickness responses in our experiments (i.e., the largest response in CESM1, which has the thickest mean sea ice, and the smallest response in CM2.1, which has the thinnest mean sea ice).

Our multimodel large ensemble experiments show a consistent and statistically significant weakening of the BSH. Several previous studies have investigated the atmospheric response to AMV-related surface temperature anomalies, but they report disparate results in the Arctic. For example, Omrani et al. (2014) present an AMV-based composite of the Hadley Centre SLP (Rayner et al. 2003) that exhibits a comparable pattern to ours (i.e., weaker Aleutian low and BSH during AMV+), but their patterns are not statistically significant (see their Fig. 2b). In a more recent study that includes composite analysis of long coupled simulations (Omrani et al. 2016), we can infer positive SLP anomalies over the Arctic (see their Fig. 2) during AMV+, which contrasts with our findings as well as with their earlier observationally based analysis. In another study, Peings and Magnusdottir (2014) show a composite using 20CR SLP (Compo et al. 2011) that suggests a weaker Aleutian low during AMV+, but a stronger yet statistically insignificant BSH (see their Fig. 2a). More recently, using atmosphere-only simulations, Peings and Magnusdottir (2016) associate Atlantic warming with a weaker Aleutian low and weaker BSH—similar to our findings—but the Arctic SLP anomalies are not statistically significant (see their Fig. 2c). Several studies have also detailed how sea ice loss is important in determining the large-scale atmospheric circulation response, and how regional sea ice loss can trigger atmospheric response that project onto known patterns of variability such as the PNA and NAO (e.g., Screen 2017).

The disparate results from previous studies along with the ability of sea ice loss to trigger atmospheric circulation responses, which could further amplify or damp atmospheric teleconnections such as the AMV-related teleconnections described in our analysis, underscore

the difficulties associated with impacts studies and the sensitivities of such studies to model configuration and experimental setup. We also contend that it emphasizes the importance of using fully coupled models with a more complete set of feedbacks to obtain a more comprehensive picture of Arctic responses/changes to AMV forcing. Such difficulties of regional impact attributions and the underlying driving mechanisms involved in long time scale variability are an outstanding issue in the decadal prediction community. The identification of robust regional impacts associated with modes of decadal variability and the understanding of the physical processes driving those impacts are often seen as vital for our ability to make reliable and skillful decadal predictions. The protocol described in RR17 and in this manuscript has been included among the proposed simulations (Component C) of the Decadal Climate Prediction Project (DCPP) Model Intercomparison Project (MIP) (Boer et al. 2016), which is an endorsed MIP of phase 6 of the Coupled Model Intercomparison Project (CMIP6; Eyring et al. 2016). The Component C experiments involve case studies of particular climate shifts and variations, including AMV, and aim to facilitate improved understanding of the underlying physical processes. As such, these coordinated simulations are expected to clarify robust aspects, reconciling the disparate results found in the literature.

Many previous studies suggest that AMOC drives a substantial fraction of the low-frequency variability of the Arctic sea ice extent (e.g., Mahajan et al. 2011; Day et al. 2012; Zhang 2015). A recent study by Delworth et al. (2016) provides further evidence for this mechanism, showing that multidecadal variations in the NAO can have broad impacts on Northern Hemisphere climate, and Arctic sea ice in particular, through its influence on AMOC and associated northward ocean heat transport into the North Atlantic and Arctic. Their results suggest that AMOC variations contributed to the rapid loss of Arctic sea ice since the late 1990s. Yeager et al. (2015) also present strong evidence that the rapid Arctic sea ice loss observed between about 1997 and 2007 was related to anomalous Atlantic Ocean heat transport based on an analysis of the CESM initialized decadal prediction system. Our results suggest that the AMV, which has been in a positive phase since 1995 (Ting et al. 2009), has also likely contributed to the observed accelerated rate of September Arctic sea ice decline since the late 1990s through atmospheric pathways. Our findings are consistent with previous studies that have linked variability and trends in ice motion, ice extent, and ice export to decadal shifts in atmospheric circulation patterns (e.g., Proshutinsky and Johnson 1997; Deser et al. 2000; Bitz et al. 2002; Rigor et al.

2002; Vihma et al. 2012). Our results show that the atmosphere-driven changes in sea ice linked to the AMV tend to be more pan-Arctic with maximum expressions in the Pacific sector, whereas changes linked to the Atlantic Ocean heat transport are more confined to the Atlantic sector (e.g., Zhang 2015; Yeager et al. 2015; Delworth et al. 2016). The present results also imply that atmospheric teleconnections might be expected to explain some of, or perhaps augment, the Arctic response to AMV associated with multidecadal variations in ocean circulation highlighted by other authors (e.g., Mahajan et al. 2011; Day et al. 2012; Zhang 2015; Delworth and Zeng 2016). For example, the strengthening of the transpolar drift drives a small increase in sea ice concentration in the Greenland Sea, where the Fram Strait represents a choke point, in our simulations. This small increase in sea ice concentration is marginally significant and in agreement with Zhang (2015). Nonetheless, this small increase in sea ice concentration would tend to lessen the impacts linked to the Atlantic Ocean heat transport.

Several recent studies have shown that the extreme loss of Arctic sea ice in the twenty-first century has been accompanied by a shift of the Arctic atmospheric circulation patterns (e.g., Wu et al. 2006; Zhang et al. 2008; Overland and Wang 2010). Since the 2000s, an SLP/wind pattern known as the AD pattern has been more prevalent in spring. Our results indicate that positive AMV SST anomalies can lead to the emergence of such a dipole pattern and suggest that the more frequent AD pattern observed since the 2000s could be partially attributed to the concurrent AMV warm phase.

To further evaluate the importance of the simulated AMV-related Arctic sea ice impacts, we compare the sea ice changes simulated in our idealized experiments with the long-term observed Arctic sea ice trend. The modern satellite passive microwave radiometers record provides us with a comprehensive estimate of the Arctic sea ice extent and area since 1979. Here, we use the September Arctic sea ice concentration from the Climate Data Record of Passive Microwave Sea Ice Concentration (Peng et al. 2013; Meier et al. 2017) provided by the NOAA National Snow and Ice Data Center (NSIDC) to compute the September Arctic Ocean sea ice area; the Arctic Ocean is defined following Holland et al. (2010). Because long-term observations of changes in ice thickness and volume are not currently available, we employ the Pan-Arctic Ice Ocean Modeling and Assimilation System (PIOMAS; Zhang and Rothrock 2003) to obtain estimates of the Arctic sea ice volume, complementing the satellite-derived sea ice area over the same 1979–2017 time period. PIOMAS has been shown to agree well with a range of observations (Schweiger et al. 2011).

Using the monthly PIOMAS ice thickness, we estimate the Arctic Ocean ice volume trend to be about $-2400 \pm 200 \text{ km}^3$ per decade over the 1979–2017 period, representing a loss of nearly 15% of the Arctic Ocean sea ice volume per decade. Over the same period, the observed trend in September Arctic Ocean sea ice area loss has been $576\,500 \pm 60\,000 \text{ km}^2$ per decade, meaning that more than 11% of the September Arctic Ocean sea ice area is lost every 10 years. The trend reflects the response of the system to anthropogenic forcing as well as to internal variability. Given that the strong influence of internal variability seen in short historical trends is greatly reduced by computing the historical trends over a 39-yr period (Swart et al. 2015), we assume that the 39-yr historical trends of sea ice area and volume reflect the response to anthropogenic forcing. Using our idealized experiments, we assume a linear response and evaluate the AMV-related decadal trends in Arctic sea ice volume and September sea ice area per AMV standard deviation as the ensemble-mean decadal trend of these fields' composite difference between AMV+ and AMV-, divided by 2. We obtain decadal trends in Arctic Ocean sea ice volume per standard deviation of the AMV index of -1.25% for CM2.1 and FLOR, and -2.5% for CESM1. The decadal trends in September sea ice area per standard deviation of the AMV index are 2.4% for CESM1 and 1% for both FLOR and CM2.1. Based on the simulated trends above, we estimate that the mechanisms described in this study could contribute to decadal modulations of the reconstructed long-term Arctic sea ice volume decline on the order of 8% – 16% for a step change of one standard deviation in AMV.⁵ We further estimate that a step change of one standard deviation in AMV could result in modulation of the long-term observed trend in September sea ice area decline on the order of 9% – 21% .

In addition to the experiments analyzed above, we have performed supplementary simulations with CESM1 and CM2.1 to investigate the respective contributions of the tropical and subpolar parts of the AMV (see RR17 for details). Our analysis reveals that neither the tropical- nor the extratropical-only experiments in either model show the Arctic sea ice thickness responses presented above (Fig. 14). The weakening of the BSH seen in Fig. 8 is also absent from the tropical- and extratropical-only experiments (not shown), and CESM1 does not show a significant response in the frequency of

⁵ The AMV index in the late 1990s was characterized by a steep change from a standard deviation of -1.17 to 0.42 over a 5-yr period. This is a shift of about 1.5 standard deviation in just 5 years, which can be qualitatively described as a step change.

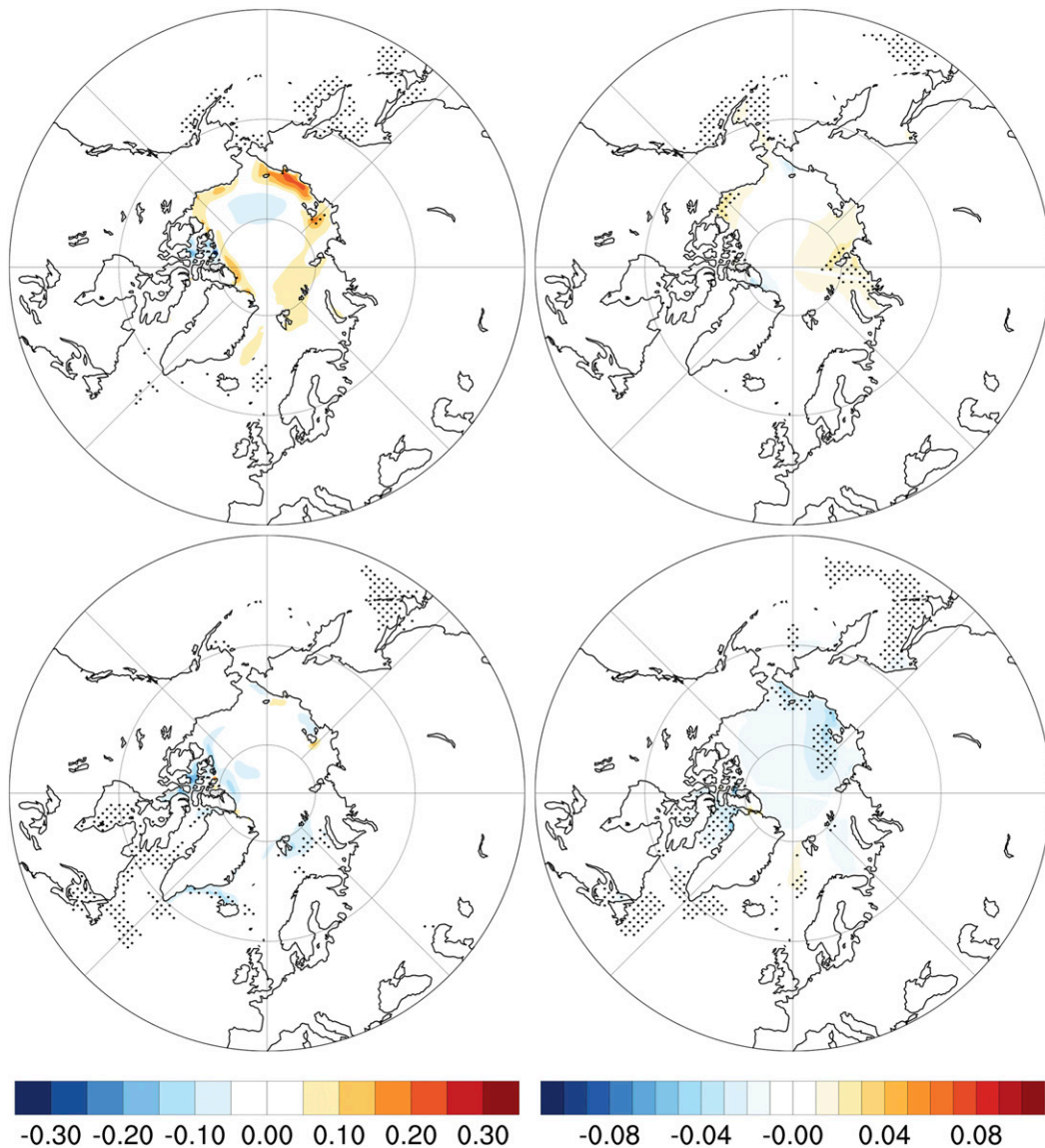


FIG. 14. Differences in 10-yr winter (DJFM) average sea ice thicknesses (m) between the AMV+ and AMV– ensemble simulations for (left) CESM1 and (right) CM2.1, for the (top) tropical-only and (bottom) subpolar-only AMV experiments. Note the different scales between the panels. Stippling indicates regions that are significant above the 95% confidence level based on a two-sided Student's t test.

winter Arctic anticyclones and northeastern North Pacific cyclones (not shown). These findings suggest that the Arctic sea ice changes associated with the AMV-induced atmospheric teleconnections are more nonlinear than the IPO response described in RR17, insofar as the Pacific SST response is largely recovered by summing the contributions from the tropical- and extratropical-only experiments. Further investigation of this apparent nonlinearity will be the subject of a future study.

Anthropogenic warming will cause Arctic sea ice to decline in the long term, but internal climate variability

can be expected to introduce significant spread in sea ice trends on decadal time scales (Kay et al. 2011). Our results suggest that decadal variations in Arctic sea ice thickness and extent may be related to the surface footprint of large internal climate variations in the Atlantic Ocean. Thus, in addition to the predictive skill in ice extent in the Atlantic sector linked to the Atlantic Ocean heat transport found in previous studies, the AMV could give rise to some predictive skill of the low-frequency modulation of the rate of pan-Arctic sea ice decline.

Acknowledgments. We are grateful to Dr. David Bailey for helpful suggestions with the CESM1 sea-ice component and analysis of its solutions. We also thank Dr. Marika Holland for insightful discussions about the Arctic sea ice dynamics and for her comments on an earlier version of the manuscript. We also thank three anonymous reviewers for their helpful suggestions, which greatly helped to improve the quality of this manuscript. This work is supported by the National Science Foundation (NSF) Collaborative Research EaSM2 Grant OCE-1243015 to NCAR and by the National Oceanic and Atmospheric Administration (NOAA) Climate Program Office Climate Variability and Predictability Program Grant NA13OAR4310138 to NCAR and GFDL. NCAR is sponsored by the NSF. All model outputs used in this study are available upon request by contacting the corresponding author.

REFERENCES

- Bitz, C. M., and G. H. Roe, 2004: A mechanism for the high rate of sea-ice thinning in the Arctic Ocean. *J. Climate*, **17**, 3623–3631, [https://doi.org/10.1175/1520-0442\(2004\)017<3623:AMFTHR>2.0.CO;2](https://doi.org/10.1175/1520-0442(2004)017<3623:AMFTHR>2.0.CO;2).
- , J. C. Fyfe, and G. M. Flato, 2002: Sea ice response to wind forcing from AMIP models. *J. Climate*, **15**, 522–536, [https://doi.org/10.1175/1520-0442\(2002\)015<0522:SIRTWF>2.0.CO;2](https://doi.org/10.1175/1520-0442(2002)015<0522:SIRTWF>2.0.CO;2).
- Blanchard-Wrigglesworth, E., K. C. Armour, C. M. Bitz, and E. DeWeaver, 2011: Persistence and inherent predictability of Arctic sea ice in a GCM ensemble and observations. *J. Climate*, **24**, 231–250, <https://doi.org/10.1175/2010JCLI3775.1>.
- Boer, G., and Coauthors, 2016: The Decadal Climate Prediction Project (DCPP) contribution to CMIP6. *Geosci. Model Dev.*, **9**, 3751–3777, <https://doi.org/10.5194/gmd-9-3751-2016>.
- Chevallier, M., and D. Salas-Méla, 2012: The role of sea ice thickness distribution in the Arctic sea ice potential predictability: A diagnostic approach with a coupled GCM. *J. Climate*, **25**, 3025–3038, <https://doi.org/10.1175/JCLI-D-11-00209.1>.
- Comiso, J. C., C. L. Parkinson, R. Gersten, and L. Stock, 2008: Accelerated decline in the Arctic sea ice cover. *Geophys. Res. Lett.*, **35**, L01703, <https://doi.org/10.1029/2007GL031972>.
- Compo, G. P., and Coauthors, 2011: The Twentieth Century Reanalysis Project. *Quart. J. Roy. Meteor. Soc.*, **137**, 1–28, <https://doi.org/10.1002/qj.776>.
- Curry, J. A., J. L. Schramm, and E. E. Elbert, 1995: Sea ice–albedo climate feedback mechanism. *J. Climate*, **8**, 240–247, [https://doi.org/10.1175/1520-0442\(1995\)008<0240:SIACFM>2.0.CO;2](https://doi.org/10.1175/1520-0442(1995)008<0240:SIACFM>2.0.CO;2).
- Day, J. J., J. C. Hargreaves, J. D. Annan, and A. Abe-Ouchi, 2012: Sources of multi-decadal variability in Arctic sea ice extent. *Environ. Res. Lett.*, **7**, 034011, <https://doi.org/10.1088/1748-9326/7/3/034011>.
- , E. Hawkins, and S. Tietsche, 2014: Will Arctic sea ice thickness initialization improve seasonal forecast skill? *Geophys. Res. Lett.*, **41**, 7566–7575, <https://doi.org/10.1002/2014GL061694>.
- Delworth, T. L., and F. Zeng, 2016: The impact of the North Atlantic Oscillation on climate through its influence on the Atlantic meridional overturning circulation. *J. Climate*, **29**, 941–962, <https://doi.org/10.1175/JCLI-D-15-0396.1>.
- , and Coauthors, 2006: GFDL’s CM2 global coupled climate models. Part I: Formulation and simulation characteristics. *J. Climate*, **13**, 643–674, <https://doi.org/10.1175/JCLI3629.1>.
- , F. Zeng, G. A. Vecchi, X. Yang, L. Zhang, and R. Zhang, 2016: The North Atlantic Oscillation as a driver of rapid climate change in the Northern Hemisphere. *Nat. Geosci.*, **9**, 509–512, <https://doi.org/10.1038/ngeo2738>.
- Deser, C., J. E. Walsh, and M. S. Timlin, 2000: Arctic sea ice variability in the context of recent atmospheric circulation trends. *J. Climate*, **13**, 617–633, [https://doi.org/10.1175/1520-0442\(2000\)013<0617:ASIVIT>2.0.CO;2](https://doi.org/10.1175/1520-0442(2000)013<0617:ASIVIT>2.0.CO;2).
- Ding, Q., and Coauthors, 2017: Influence of high-latitude atmospheric circulation changes on summertime Arctic sea ice. *Nat. Climate Change*, **7**, 289–295, <https://doi.org/10.1038/nclimate3241>.
- Dong, B., R. T. Sutton, and A. A. Scaife, 2006: Multidecadal modulation of El Niño–Southern Oscillation (ENSO) variance by Atlantic Ocean sea surface temperatures. *Geophys. Res. Lett.*, **33**, L08705, <https://doi.org/10.1029/2006GL025766>.
- Döscher, R., T. Vihma, and E. Maksimovich, 2014: Recent advances in understanding the Arctic climate system state and change from a sea ice perspective: A review. *Atmos. Chem. Phys.*, **14**, 13 571–13 600, <https://doi.org/10.5194/acp-14-13571-2014>.
- Emery, W. J., C. W. Fowler, and J. A. Maslanik, 1997: Satellite-derived maps of Arctic and Antarctic sea ice motion 1988 to 1994. *Geophys. Res. Lett.*, **24**, 897–900, <https://doi.org/10.1029/97GL00755>.
- Eyring, V., S. Bony, G. A. Meehl, C. A. Senior, B. Stevens, R. J. Stouffer, and K. E. Taylor, 2016: Overview of the Coupled Model Intercomparison Project phase 6 (CMIP6) experimental design and organization. *Geosci. Model Dev.*, **9**, 1937–1958, <https://doi.org/10.5194/gmd-9-1937-2016>.
- Griffies, S. M., and Coauthors, 2011: The GFDL CM3 coupled climate model: Characteristics of the ocean and sea ice simulations. *J. Climate*, **24**, 3520–3544, <https://doi.org/10.1175/2011JCLI3964.1>.
- Guemas, V., and Coauthors, 2016: A review on Arctic sea-ice predictability and prediction on seasonal to decadal time-scales. *Quart. J. Roy. Meteor. Soc.*, **142**, 546–561, <https://doi.org/10.1002/qj.2401>.
- Hansen, E., and Coauthors, 2013: Thinning of Arctic sea ice observed in Fram Strait: 1990–2011. *J. Geophys. Res. Oceans*, **118**, 5202–5221, <https://doi.org/10.1002/jgrc.20393>.
- Hawkins, E., R. S. Smith, J. M. Gregory, and D. A. Stainforth, 2016: Irreducible uncertainty in near-term climate projections. *Climate Dyn.*, **46**, 3807–3819, <https://doi.org/10.1007/s00382-015-2806-8>.
- Holland, M. M., M. C. Serreze, and J. Stroeve, 2010: The sea ice mass budget of the Arctic and its future change as simulated by coupled climate models. *Climate Dyn.*, **34**, 185–200, <https://doi.org/10.1007/s00382-008-0493-4>.
- Inoue, J., and T. Kikuchi, 2007: Outflow of summertime Arctic sea ice observed by ice drifting buoys and its linkage with ice reduction and atmospheric circulation patterns. *J. Meteor. Soc. Japan*, **85**, 881–887, <https://doi.org/10.2151/jmsj.85.881>.
- Itkin, P., and T. Krumpfen, 2017: Winter sea ice export from the Laptev Sea preconditions the local summer sea ice cover and fast ice decay. *Cryosphere*, **11**, 2383–2391, <https://doi.org/10.5194/tc-11-2383-2017>.
- Johannessen, O. M., S. I. Kuzmina, L. P. Bobylev, and M. W. Miles, 2016: Surface air temperature variability and trends in the Arctic: New amplification assessment and regionalisation. *Tellus*, **68A**, 28234, <https://doi.org/10.3402/tellusa.v68.28234>.

- Kavvada, A., A. Ruiz-Barradas, and S. Nigam, 2013: AMO's structure and climate footprint in observations and IPCC AR5 climate simulations. *Climate Dyn.*, **41**, 1345–1364, <https://doi.org/10.1007/s00382-013-1712-1>.
- Kay, J. E., and A. Gettelman, 2009: Cloud influence on and response to seasonal Arctic sea ice loss. *J. Geophys. Res.*, **114**, D18204, <https://doi.org/10.1029/2009JD011773>.
- , M. M. Holland, and A. Jahn, 2011: Inter-annual to multi-decadal Arctic sea ice extent trends in a warming world. *Geophys. Res. Lett.*, **38**, L15708, <https://doi.org/10.1029/2011GL048008>.
- , and Coauthors, 2015: The Community Earth System Model (CESM) large ensemble project: A community resource for studying climate change in the presence of internal climate variability. *Bull. Amer. Meteor. Soc.*, **96**, 1333–1349, <https://doi.org/10.1175/BAMS-D-13-00255.1>.
- Knight, J. R., C. K. Folland, and A. A. Scaife, 2006: Climate impacts of the Atlantic multidecadal oscillation. *Geophys. Res. Lett.*, **33**, L17706, <https://doi.org/10.1029/2006GL026242>.
- Kwok, R., 2011: Observational assessment of Arctic Ocean sea ice motion, export, and thickness in CMIP3 climate simulations. *J. Geophys. Res.*, **116**, C00D05, <https://doi.org/10.1029/2011JC007004>.
- , G. Spreen, and S. Pang, 2013: Arctic sea ice circulation and drift speed: Decadal trends and ocean currents. *J. Geophys. Res. Oceans*, **118**, 2408–2425, <https://doi.org/10.1002/jgrc.20191>.
- Langehaug, H. R., F. Geyer, L. H. Smedsrud, and Y. Gao, 2013: Arctic sea ice decline and ice export in the CMIP5 historical simulations. *Ocean Modell.*, **71**, 114–126, <https://doi.org/10.1016/j.oceanmod.2012.12.006>.
- L'Heureux, M. L., A. Kumar, G. D. Bell, M. S. Halpert, and R. W. Higgins, 2008: Role of the Pacific–North American (PNA) pattern in the 2007 Arctic sea ice decline. *Geophys. Res. Lett.*, **35**, L20701, <https://doi.org/10.1029/2008GL035205>.
- Mahajan, S., R. Zhang, and T. L. Delworth, 2011: Impact of the Atlantic meridional overturning circulation (AMOC) on Arctic surface air temperature and sea ice variability. *J. Climate*, **24**, 6573–6581, <https://doi.org/10.1175/2011JCLI4002.1>.
- Maslanik, J., S. Drobot, C. Fowler, W. Emery, and R. Barry, 2007: On the Arctic climate paradox and the continuing role of atmospheric circulation in affecting sea ice conditions. *Geophys. Res. Lett.*, **34**, L03711, <https://doi.org/10.1029/2006GL028269>.
- Meier, W., F. Fetterer, M. Savoie, S. Mallory, R. Duerr, and J. Stroeve, 2017: NOAA/NSIDC climate data record of passive microwave sea ice concentration, version 3. National Snow and Ice Data Center, accessed 14 September 2018, <https://doi.org/10.7265/N59P2ZTG>.
- Miles, M. W., D. V. Divine, T. Furevik, E. Jansen, M. Moros, and A. E. J. Ogilvie, 2014: A signal of persistent Atlantic multidecadal variability in Arctic sea ice. *Geophys. Res. Lett.*, **41**, 463–469, <https://doi.org/10.1002/2013GL058084>.
- Morrison, H., G. De Boer, G. Feingold, J. Harrington, M. D. Shupe, and K. Sulia, 2012: Resilience of persistent Arctic mixed-phase clouds. *Nat. Geosci.*, **5**, 11–17, <https://doi.org/10.1038/ngeo1332>.
- Nghiem, S. V., I. G. Rigor, D. K. Perovich, P. Clemente-Colón, J. W. Weatherly, and G. Neumann, 2007: Rapid reduction of Arctic perennial sea ice. *Geophys. Res. Lett.*, **34**, L19504, <https://doi.org/10.1029/2007GL031138>.
- Ogi, M., and I. G. Rigor, 2013: Trends in Arctic sea ice and the role of atmospheric circulation. *Atmos. Sci. Lett.*, **14**, 97–101, <https://doi.org/10.1002/asl2.423>.
- Omriani, N. E., N. S. Keenlyside, J. Bader, and E. Manzini, 2014: Stratosphere key for wintertime atmospheric response to warm Atlantic decadal conditions. *Climate Dyn.*, **42**, 649–663, <https://doi.org/10.1007/s00382-013-1860-3>.
- , —, —, and —, 2016: Troposphere–stratosphere response to large-scale North Atlantic Ocean variability in an atmosphere/ocean coupled model. *Climate Dyn.*, **46**, 1397–1415, <https://doi.org/10.1007/s00382-015-2654-6>.
- Overland, J. E., and M. Wang, 2010: Large-scale atmospheric circulation changes are associated with the recent loss of Arctic sea ice. *Tellus*, **62A**, 1–9, <https://doi.org/10.1111/j.1600-0870.2009.00421.x>.
- Peings, Y., and G. Magnusdottir, 2014: Forcing of the wintertime atmospheric circulation by the multidecadal fluctuations of the North Atlantic Ocean. *Environ. Res. Lett.*, **9**, 034018, <https://doi.org/10.1088/1748-9326/9/3/034018>.
- , and —, 2016: Wintertime atmospheric response to Atlantic multidecadal variability: Effect of stratospheric representation and ocean–atmosphere coupling. *Climate Dyn.*, **47**, 1029–1047, <https://doi.org/10.1007/s00382-015-2887-4>.
- Peng, G., W. Meier, D. Scott, and M. Savoie, 2013: A long-term and reproducible passive microwave sea ice concentration data record for climate studies and monitoring. *Earth Syst. Sci. Data*, **5**, 311–318, <https://doi.org/10.5194/essd-5-311-2013>.
- Pickart, R. S., A. M. Macdonald, G. W. Moore, I. A. Renfrew, J. E. Walsh, and W. S. Kessler, 2009: Seasonal evolution of Aleutian low pressure systems: Implications for the North Pacific subpolar circulation. *J. Phys. Oceanogr.*, **39**, 1317–1339, <https://doi.org/10.1175/2008JPO3891.1>.
- Pithan, F., and T. Mauritsen, 2014: Arctic amplification dominated by temperature feedbacks in contemporary climate models. *Nat. Geosci.*, **7**, 181–184, <https://doi.org/10.1038/ngeo2071>.
- Polyakov, I. V., J. E. Walsh, and R. Kwok, 2012: Recent changes of Arctic multiyear sea ice coverage and the likely causes. *Bull. Amer. Meteor. Soc.*, **93**, 145–151, <https://doi.org/10.1175/BAMS-D-11-00070.1>.
- Proshutinsky, A. Y., and M. A. Johnson, 1997: Two circulation regimes of the wind-driven Arctic Ocean. *J. Geophys. Res.*, **102**, 12 493–12 514, <https://doi.org/10.1029/97JC00738>.
- Rampal, P., J. Weiss, and D. Marsan, 2009: Positive trend in the mean speed and deformation rate of Arctic sea ice, 1979–2007. *J. Geophys. Res.*, **114**, C05013, <https://doi.org/10.1029/2008JC005066>.
- , —, C. Dubois, and J.-M. Campin, 2011: IPCC climate models do not capture Arctic sea ice drift acceleration: Consequences in terms of projected sea ice thinning and decline. *J. Geophys. Res.*, **116**, C00D07, <https://doi.org/10.1029/2011JC007110>.
- Rayner, N. A., D. E. Parker, E. B. Horton, C. K. Folland, L. V. Alexander, D. P. Rowell, E. C. Kent, and A. Kaplan, 2003: Global analyses of sea surface temperature, sea ice, and night marine air temperature since the late nineteenth century. *J. Geophys. Res.*, **108**, 4407, <https://doi.org/10.1029/2002JD002670>.</jrn
- Rigor, I. G., J. M. Wallace, and R. L. Colony, 2002: Response of sea ice to the Arctic Oscillation. *J. Climate*, **15**, 2648–2663, [https://doi.org/10.1175/1520-0442\(2002\)015<2648:ROSITT>2.0.CO;2](https://doi.org/10.1175/1520-0442(2002)015<2648:ROSITT>2.0.CO;2).
- Ruprich-Robert, Y., R. Msadek, F. Castruccio, S. Yeager, T. Delworth, and G. Danabasoglu, 2017: Assessing the climate impacts of the observed Atlantic multidecadal variability using the GFDL CM2.1 and NCAR CESM1 global coupled models. *J. Climate*, **30**, 2785–2810, <https://doi.org/10.1175/JCLI-D-16-0127.1>.

- Schweiger, A., R. Lindsay, J. Zhang, M. Steele, H. Stern, and R. Kwok, 2011: Uncertainty in modeled Arctic sea ice volume. *J. Geophys. Res.*, **116**, C00D06, <https://doi.org/10.1029/2011JC007084>.
- Screen, J. A., 2017: Simulated atmospheric response to regional and Pan-Arctic sea ice loss. *J. Climate*, **30**, 3945–3962, <https://doi.org/10.1175/JCLI-D-16-0197.1>.
- , and I. Simmonds, 2010: The central role of diminishing sea ice in recent Arctic temperature amplification. *Nature*, **464**, 1334–1337, <https://doi.org/10.1038/nature09051>.
- , —, and K. Keay, 2011: Dramatic interannual changes of perennial Arctic sea ice linked to abnormal summer storm activity. *J. Geophys. Res.*, **116**, D15105, <https://doi.org/10.1029/2011JD015847>.
- Serreze, M. C., and A. P. Barrett, 2011: Characteristics of the Beaufort Sea high. *J. Climate*, **24**, 159–182, <https://doi.org/10.1175/2010JCLI3636.1>.
- Shupe, M. D., and J. M. Intrieri, 2004: Cloud radiative forcing of the arctic surface: The influence of cloud properties, surface albedo, and solar zenith angle. *J. Climate*, **17**, 616–628, [https://doi.org/10.1175/1520-0442\(2004\)017<0616:CRFOTA>2.0.CO;2](https://doi.org/10.1175/1520-0442(2004)017<0616:CRFOTA>2.0.CO;2).
- Simmonds, I., and K. Keay, 2009: Extraordinary September Arctic sea ice reductions and their relationships with storm behavior over 1979–2008. *Geophys. Res. Lett.*, **36**, L19715, <https://doi.org/10.1029/2009GL039810>.
- Smedsrud, L. H., M. H. Halvorsen, J. C. Stroeve, R. Zhang, and K. Kloster, 2017: Fram Strait sea ice export variability and September Arctic sea ice extent over the last 80 years. *Cryosphere*, **11**, 65–79, <https://doi.org/10.5194/tc-11-65-2017>.
- Smith, T. M., R. W. Reynolds, T. C. Peterson, and J. Lawrimore, 2008: Improvements to NOAA's historical merged land-ocean surface temperature analysis (1880–2006). *J. Climate*, **21**, 2283–2296, <https://doi.org/10.1175/2007JCLI2100.1>.
- Soden, B. J., I. M. Held, R. Colman, K. M. Shell, J. T. Kiehl, and C. A. Shields, 2008: Quantifying climate feedbacks using radiative kernels. *J. Climate*, **21**, 3504–3520, <https://doi.org/10.1175/2007JCLI2110.1>.
- Stroeve, J. C., M. M. Holland, W. Meier, T. Scambos, and M. Serreze, 2007: Arctic sea ice decline: Faster than forecast. *Geophys. Res. Lett.*, **24**, L09501, <https://doi.org/10.1029/2007GL029703>.
- , J. Maslanik, M. C. Serreze, I. Rigor, W. Meier, and C. Fowler, 2011: Sea ice response to an extreme negative phase of the Arctic Oscillation during winter 2009/2010. *Geophys. Res. Lett.*, **38**, L02502, <https://doi.org/10.1029/2010GL045662>.
- , V. Kattsov, A. Barrett, M. Serreze, T. Pavlova, M. Holland, and W. N. Meier, 2012: Trends in Arctic sea ice extent from CMIP5, CMIP3 and observations. *Geophys. Res. Lett.*, **39**, L16502, <https://doi.org/10.1029/2012GL052676>.
- Sung, M.-K., S.-I. An, B.-M. Kim, and S.-H. Woo, 2014: A physical mechanism of the precipitation dipole in the western United States based on PDO–storm track relationship. *Geophys. Res. Lett.*, **41**, 4719–4726, <https://doi.org/10.1002/2014GL060711>.
- Sutton, R. T., and D. L. R. Hodson, 2005: Atlantic Ocean forcing of North American and European summer climate. *Science*, **309**, 115–118, <https://doi.org/10.1126/science.1109496>.
- Swart, N. C., J. C. Fyfe, E. Hawkins, J. E. Kay, and A. Jahn, 2015: Influence of internal variability on Arctic sea-ice trends. *Nat. Climate Change*, **5**, 86–89, <https://doi.org/10.1038/nclimate2483>.
- Thompson, D. W. J., and J. M. Wallace, 1998: The Arctic Oscillation signature in the wintertime geopotential height and temperature fields. *Geophys. Res. Lett.*, **25**, 1297–1300, <https://doi.org/10.1029/98GL00950>.
- Ting, M., Y. Kushnir, R. Seager, and C. Li, 2009: Forced and internal twentieth-century SST trends in the North Atlantic. *J. Climate*, **22**, 1469–1481, <https://doi.org/10.1175/2008JCLI2561.1>.
- Uttal, T., and Coauthors, 2002: Surface heat budget of the Arctic Ocean. *Bull. Amer. Meteor. Soc.*, **83**, 255–276, [https://doi.org/10.1175/1520-0477\(2002\)083<0255:SHBOTA>2.3.CO;2](https://doi.org/10.1175/1520-0477(2002)083<0255:SHBOTA>2.3.CO;2).
- Vecchi, G. A., and Coauthors, 2014: On the seasonal forecasting of regional tropical cyclone activity. *J. Climate*, **27**, 7994–8016, <https://doi.org/10.1175/JCLI-D-14-00158.1>.
- Vihma, T., P. Tisler, and P. Uotila, 2012: Atmospheric forcing on the drift of Arctic sea ice in 1989–2009. *Geophys. Res. Lett.*, **39**, L02501, <https://doi.org/10.1029/2011GL050118>.
- Wernli, H., and L. Papritz, 2018: Role of polar anticyclones and mid-latitude cyclones for Arctic summertime sea-ice melting. *Nat. Geosci.*, **11**, 108–113, <https://doi.org/10.1038/s41561-017-0041-0>.
- Wu, B., J. Wang, and J. E. Walsh, 2006: Dipole anomaly in the winter Arctic atmosphere and its association with sea ice motion. *J. Climate*, **19**, 210–225, <https://doi.org/10.1175/JCLI3619.1>.
- Yeager, S. G., A. R. Karspeck, and G. Danabasoglu, 2015: Predicted slowdown in the rate of Atlantic sea ice loss. *Geophys. Res. Lett.*, **42**, 10 704–10 713, <https://doi.org/10.1002/2015GL065364>.
- Yu, L., S. Zhong, J. A. Winkler, M. Zhou, D. H. Lenschow, B. Li, X. Wang, and Q. Yang, 2017: Possible connections of the opposite trends in Arctic and Antarctic sea-ice cover. *Sci. Rep.*, **7**, 45804, <https://doi.org/10.1038/srep45804>.
- Zhang, J. L., and D. A. Rothrock, 2003: Modeling global sea ice with a thickness and enthalpy distribution model in generalized curvilinear coordinates. *Mon. Wea. Rev.*, **131**, 845–861, [https://doi.org/10.1175/1520-0493\(2003\)131<0845:MGSIWA>2.0.CO;2](https://doi.org/10.1175/1520-0493(2003)131<0845:MGSIWA>2.0.CO;2).
- Zhang, R., 2015: Mechanisms for low-frequency variability of summer Arctic sea ice extent. *Proc. Natl. Acad. Sci. USA*, **112**, 4570–4575, <https://doi.org/10.1073/pnas.1422296112>.
- , and T. L. Delworth, 2006: Impact of Atlantic multidecadal oscillations on India/Sahel rainfall and Atlantic hurricanes. *Geophys. Res. Lett.*, **33**, L17712, <https://doi.org/10.1029/2006GL026267>.
- , and —, 2007: Impact of the Atlantic multidecadal oscillation on North Pacific climate variability. *Geophys. Res. Lett.*, **34**, L23708, <https://doi.org/10.1029/2007GL031601>.
- Zhang, X., A. Sorteberg, J. Zhang, R. Gerdes, and J. C. Comiso, 2008: Recent radical shifts of atmospheric circulations and rapid changes in Arctic climate system. *Geophys. Res. Lett.*, **35**, L22701, <https://doi.org/10.1029/2008GL035607>.